initiate hyperphosphorylation. But as it has generally been observed, high phosphorylation of Tau increases its propensity to dissociate from microtubules (9, 11). Compared with mutant Tau proteins, P-WT Tau, upon dissociation from microtubules, is dephosphorylated easily after conversion to the *trans* form by Pin1, and therefore WT Tau is much less likely to form aggregates *i.e.* representing the non-pathologic state.

REFERENCES

1. Lee, V. M., Goedert, M., and Trojanowski, J. Q. (2001) *Annu. Rev. Neurosci.* **24,** 1121–1159
2. Goedert, M., and Spillantini, M. G. (2006) *Science* **314,** 777–781
3. Hasegawa, M. (2006) *Neuropathology* **26,** 484–490
4. Hutton, M., Lendon, C. L., Rizzu, P., Baker, M., Froelich, S., Houlden, H., Pickering-Brown, S., Chakraverty, S., Isaacs, A., Grover, A., Hackett, J., Adamson, J., Lincoln, S., Dickson, D., Davies, P., Petersen, R. C., Stevens, M., de Graaff, E., Wauters, E., van Baren, J., Hillebrand, M., Joosse, M., Kwon, J. M., Nowotny, P., Che, L. K., Norton, J., Morris, J. C., Reed, L. A., Trojanowski, J., Basun, H., Lannfelt, L., Neystat, M., Fahn, S., Dark, F., Tannenberg, T., Dodd, P. R., Hayward, N., Kwok, J. B., Schofield, P. R., Andreadis, A., Snowden, J., Craufurd, D., Neary, D., Owen, F., Oostra, B. A., Hardy, J., Goate, A., van Swieten, J., Mann, D., Lynch, T., and Heutink, P. (1998) *Nature* **393,** 702–705
5. Poorkaj, P., Bird, T. D., Wijsman, E., Nemens, E., Garruto, R. M., Anderson, L., Andreadis, A., Wiederholt, W. C., Raskind, M., and Schellenberg, G. D. (1998) *Ann. Neurol.* **43,** 815–825
6. Spillantini, M. G., Crowther, R. A., Jakes, R., Hasegawa, M., and Goedert, M. (1998) *Proc. Natl. Acad. Sci. U. S. A.* **95,** 6469–6473
7. Morishima-Kawashima, M., Hasegawa, M., Takio, K., Suzuki, M., Yoshida, H., Titani, K., and Ihara, Y. (1995) *J. Biol. Chem.* **270,** 823–829
8. Hanger, D. P., Betts, J. C., Loviny, T. L., Blackstock, W. P., and Anderton, B. H. (1998) *J. Neurochem.* **71,** 2465–2476
9. Mandelkow, E. M., Biernat, J., Drewes, G., Gustke, N., Trinczek, B., and Mandelkow, E. (1995) *Neurobiol. Aging* **16,** 355–362, discussion 362–363
10. Imahori, K., and Uchida, T. (1997) *J. Biochem.* **121,** 179–188
11. Iqbal, K., Alonso Adel, C., Chen, S., Chohan, M. O., El-Akkad, E., Gong, C. X., Khatoon, S., Li, B., Liu, F., Rahman, A., Tanimukai, H., and Grundke-Iqbal, I. (2005) *Biochim. Biophys. Acta* **1739,** 198–210
12. Avila, J. (2006) *FEBS Lett.* **580,** 2922–2927
13. Matsumura, N., Yamazaki, T., and Ihara, Y. (1999) *Am. J. Pathol.* **154,** 1649–1656
14. Dayanandan, R., Van Slegtenhorst, M., Mack, T. G., Ko, L., Yen, S. H., Leroy, K., Brion, J. P., Anderton, B. H., Hutton, M., and Lovestone, S. (1999) *FEBS Lett.* **446,** 228–232
15. Pérez, M., Lim, F., Arrasate, M., and Avila, J. (2000) *J. Neurochem.* **74,** 2583–2589
16. Sahara, N., Tomiyama, T., and Mori, H. (2000) *J. Neurosci. Res.* **60,** 380–387
17. Connel, J. W., Gibb, G. M., Betts, J. C., Blackstock, W. P., Gallo, J., Lovestone, S., Hutton, M., and Anderton, B. H. (2000) *FEBS Lett.* **493,** 40–44
18. Mack, T. G., Dayanandan, R., Van Slegtenhorst, M., Whone, A., Hutton, M., Lovestone, S., and Anderton, B. H. (2001) *Neuroscience* **108,** 701–712
19. Alonso, A., del, C., Mederlyova, A., Novak, M., Grundke-Iqbal, I., and Iqbal, K. (2004) *J. Biol. Chem.* **279,** 34873–34881
20. Krishnamurthy, P. K., and Johnson, G. V. (2004) *J. Biol. Chem.* **279,** 7893–7900
21. Gong, C. X., Grundke-Iqbal, I., and Iqbal, K. (1994) *Neuroscience* **61,** 765–772
22. Goedert, M., Jakes, R., Qi, Z., Wang, J. H., and Cohen, P. (1995) *J. Neurochem.* **65,** 2804–2807
23. Kins, S., Crameri, A., Evans, D. R., Hemmings, B. A., Nitsch, R. M., and Gotz, J. (2001) *J. Biol. Chem.* **276,** 38193–38200
24. Gong, C. X., Shaikh, S., Wang, J. Z., Zaidi, T., Grundke-Iqbal, I., and Iqbal, K. (1995) *J. Neurochem.* **65,** 732–738
25. Gong, C. X., Lidsky, T., Wegiel, J., Zuck, L., Grundke-Iqbal, I., and Iqbal, K. (2000) *J. Biol. Chem.* **275,** 5535–5544
26. Sontag, E., Hladik, C., Montgomery, L., Luangpirom, A., Mudrak, I., Ogris,
27. E., and White, C. L., 3rd. (2004) *J. Neuropathol. Exp. Neurol.* **63,** 1080–1091
27. Yamamoto, H., Hasegawa, M., Ono, T., Tashima, K., Ihara, Y., and Miyamoto, E. (1995) *J. Biochem.* **118,** 1224–1231
28. Lu, K. P., and Zhou, X. Z. (2007) *Nat. Rev. Mol. Cell Biol.* **8,** 904–916
29. Takahashi, K., Uchida, C., Shin, R. W., Shimazaki, K., and Uchida, T. (2008) *Cell Mol. Life Sci.* **65,** 359–375
30. Lu, P. J., Wulf, G., Zhou, X. Z., Davies, P., and Lu, K. P. (1999) *Nature* **399,** 784–788
31. Zhou, X. Z., Kops, O., Werner, A., Lu, P.-J., Shen, M., Stoller, G., Küllertz, G., Stark, M., Fischer, G., and Lu, K. P. (2000) *Mol. Cell* **6,** 873–883
32. Smet, C., Sambo, A. V., Wieruszeski, J. M., Leroy, A., Landrieu, I., Buée, L., and Lippens, G. (2004) *Biochemistry* **43,** 2032–2040
33. Galas, M. C., Dourlen, P., Bégard, S., Ando, K., Blum, D., Hamdane, M., and Buée, L. (2006) *J. Biol. Chem.* **281,** 19296–19304
34. Lim, J., Balastik, M., Lee, T. H., Nakamura, K., Liou, Y. C., Sun, A., Finn, G., Pastorino, L., Lee, V. M., and Lu, K. P. (2008) *J. Clin. Invest.* **118,** 1877–1889
35. Sakaue, F., Saito, T., Sato, Y., Asada, A., Ishiguro, K., Hasegawa, M., and Hisanaga, S. (2005) *J. Biol. Chem.* **280,** 31522–31529
36. Akiyama, H., Shin, R. W., Uchida, C., Kitamoto, T., and Uchida, T. (2005) *Biochem. Biophys. Res. Commun.* **336,** 521–529
37. Saito, T., Onuki, R., Fujita, Y., Kusakawa, G., Ishiguro, K., Bibb, J. A., Kishimoto, T., and Hisanaga, S. (2003) *J. Neurosci.* **23,** 1189–1197
38. Sasaki, T., Taoka, M., Ishiguro, K., Uchida, A., Saito, T., Isobe, T., and Hisanaga, S. (2002) *J. Biol. Chem.* **277,** 36032–36039
39. Hasegawa, M., Smith, M. J., and Goedert, M. (1998) *FEBS Lett.* **437,** 207–210
40. Wada, Y., Ishiguro, K., Itoh, T. J., Uchida, T., Hotani, H., Saito, T., Kishimoto, T., and Hisanaga, S. (1998) *J. Biochem.* **124,** 738–746
41. Fanghänel, J., Akiyama, H., Uchida, C., and Uchida, T. (2006) *FEBS Lett.* **580,** 3237–3245
42. Schneider, A., Biernat, J., von Bergen, M., Mandelkow, E., and Mandelkow, E. M. (1999) *Biochemistry* **23,** 3549–3558
43. Amos, L. A., and Schlieper, D. (2005) *Adv. Protein Chem.* **71,** 257–298
44. Morfini, G., Pigino, G., Mizuno, N., Kikkawa, M., and Brady, S. T. (2007) *J. Neurosci. Res.* **85,** 2620–2630
45. Miyasaka, T., Morishima-Kawashima, M., Ravid, R., Heutink, P., van Swieten, J. C., Nagashima, K., and Ihara, Y. (2001) *Am. J. Path.* **158,** 373–379
46. Bird, T. D., Nochlin, D., Poorkaj, P., Cherrier, M., Kaye, J., Payami, H., Peskind, E., Lampe, T. H., Nemens, E., Boyer, P. J., and Schellenberg, G. D. (1999) *Brain* **122,** 741–756
47. van Swieten, J. C., Stevens, M., Rosso, S. M., Rizzu, P., Joosse, M., de Koning, I., Kamphorst, W., Ravid, R., Spillantini, M. G., Niermeijer, and Heutink, P. (1999) *Ann. Neurol.* **46,** 617–626
48. Reed, L. A., Grabowski, T. J., Schmidt, M. L., Morris, J. C., Goate, A., Solodkin, A., Van Hoesen, G. W., Schelper, R. L., Talbot, C. J., Wragg, M. A., and Trojanowski, J. Q. (1997) *Ann. Neurol.* **42,** 564–572
49. Rizzu, P., Joosse, M., Ravid, R., Hoogeveen, A., Kamphorst, W., van Swieten, J. C., Willemsen, R., and Heutink, P. (2000) *Hum. Mol. Genet.* **9,** 3075–3082
50. Aoyagi, H., Hasegawa, M., and Tamaoka, A. (2007) *J. Biol. Chem.* **282,** 20309–20318
51. Hong, M., Zhukareva, V., Vogelsberg-Ragaglia, V., Wszolek, Z., Reed, L., Miller, B. I., Geschwind, D. H., Bird, T. D., McKeel, D., Goate, A., Morris, J. C., Wilhelmsen, K. C., Schellenberg, G. D., Trojanowski, J. Q., and Lee, V. M. (1998) *Science.* **282,** 1914–1917
52. Bunker, J. M., Kamath, K., Wilson, L., Jordan, M. A., and Feinstein, S. C. (2006) *J. Biol. Chem.* **281,** 11856–11863
53. Han, D., and Paudel, H. K. (2009) *Neurochem Int.* **54,** 14–27
54. Cole, A. R., Soutar, M. P., Rembutsu, M., van Aalten, L., Hastie, C. J., McLauchlan, H., Peggie, M., Balastik, M., Lu, K. P., and Sutherland, C. (2008) *J. Biol. Chem.* **283,** 18227–18237
55. Tatebayashi, Y., Miyasaka, T., Chui, D. H., Akagi, T., Mishima, K., Iwasaki, K., Fujiwara, M., Tanemura, K., Murayama, M., Ishiguro, K., Planel, E., Sato, S., Hashikawa, T., and Takashima, A. (2002) *Proc. Natl. Acad. Sci. U. S. A.* **99,** 13896–13901
56. Tatebayashi, Y., Planel, E., Chui, D. H., Sato, S., Miyasaka, T., Sahara, N.,

99

Murayama, M., Kikuchi, N., Yoshioka, K., Rivka, R., and Takashima, A. (2006) *FASEB J.* **20,** 762–774

57. Otvos, L., Jr., Feiner, L., Lang, E., Szendrei, G. I., Goedert, M., and Lee, V. M. (1994) *J. Neurosci. Res.* **39,** 669–673

58. Fischer, D., Mukrasch, M. D., von Bergen, M., Klos-Witkowska, A., Biernat, J., Griesinger, C., Mandelkow, E., and Zweckstetter, M. (2007) *Biochemistry* **46,** 2574–2782

59. Wintjens, R., Wieruszeski, J. M., Drobecq, H., Rousselot-Pailley, P., Buée, L., Lippens, G., and Landrieu, I. (2001) *J. Biol. Chem.* **276,** 25150–25156

60. Sontag, E., Nunbhakdi-Craig, V., Lee, G., Brandt, R., Kamibayashi, C., Kuret, J., White, C. L., 3rd, Mumby, M. C., and Bloom, G. S. (1999) *J. Biol. Chem.* **274,** 25490–25498

61. Horowitz, P. M., LaPointe, N., Guillozet-Bongaarts, A. L., Berry, R. W., and Binder, L. I. (2006) *Biochemistry* **45,** 12859–12866

62. Jeganathan, S., von Bergen, M., Brutlach, H., Steinhoff, H. J., and Mandelkow, E. (2006) *Biochemistry* **45,** 2283–2293

63. Mukrasch, M. D., von Bergen, M., Biernat, J., Fischer, D., Griesinger, C., Mandelkow, E., and Zweckstetter, M. (2007) *J. Biol. Chem.* **282,** 12230–12239

100

PLoS one

Beneficial Effects of Estrogen in a Mouse Model of Cerebrovascular Insufficiency

Naohito Kitamura[1⑤], Runa Araya[1⑤], Moeko Kudoh[1], Haruo Kishida[1], Tetsuya Kimura[2], Miyuki Murayama[2], Akihiko Takashima[2], Yuriko Sakamaki[3], Tsutomu Hashikawa[3], Shingo Ito[4], Sumio Ohtsuki[4], Tetsuya Terasaki[4], Jürgen Wess[5], Masahisa Yamada[1]*

1 Yamada Research Unit, RIKEN Brain Science Institute, Saitama, Japan, 2 Laboratory for Alzheimer's Diseases, RIKEN Brain Science Institute, Saitama, Japan, 3 Research Resource Center, RIKEN Brain Science Institute, Saitama, Japan, 4 Department of Molecular Biopharmacy and Genetics, Tohoku University, Sendai, Japan, 5 Laboratory of Bioorganic Chemistry, National Institute of Diabetes and Digestive and Kidney Diseases, Bethesda, Maryland, United States of America

Abstract

Background: The M_5 muscarinic acetylcholine receptor is known to play a crucial role in mediating acetylcholine dependent dilation of cerebral blood vessels. Previously, we reported that male M_5 muscarinic acetylcholine knockout mice ($M5R^{-/-}$ mice) suffer from a constitutive constriction of cerebral arteries, reduced cerebral blood flow, dendritic atrophy, and short-term memory loss, without necrosis and/or inflammation in the brain.

Methodology/Principal Findings: We employed the Magnetic Resonance Angiography to study the area of the basilar artery in male and female $M5R^{-/-}$ mice. Here we show that female $M5R^{-/-}$ mice did not show the reduction in vascular area observed in male $M5R^{-/-}$ mice. However, ovariectomized female $M5R^{-/-}$ mice displayed phenotypic changes similar to male $M5R^{-/-}$ mice, strongly suggesting that estrogen plays a key role in the observed gender differences. We found that 17β-estradiol (E2) induced nitric oxide release and ERK activation in a conditional immortalized mouse brain cerebrovascular endothelial cell line. Agonists of ERα, ERβ, and GPR30 promoted ERK activation in this cell line. Moreover, *in vivo* magnetic resonance imaging studies showed that the cross section of the basilar artery was restored to normal in male $M5R^{-/-}$ mice treated with E2. Treatment with E2 also improved the performance of male $M5R^{-/-}$ mice in a cognitive test and reduced the atrophy of neural dendrites in the cerebral cortex and hippocampus. $M5R^{-/-}$ mice also showed astrocyte swelling in cortex and hippocampus using the three-dimensional reconstruction of electron microscope images. This phenotype was reversed by E2 treatment, similar to the observed deficits in dendrite morphology and the number of synapses.

Conclusions/Significance: Our findings indicate that $M5R^{-/-}$ mice represent an excellent novel model system to study the beneficial effects of estrogen on cerebrovascular function and cognition. E2 may offer new therapeutic perspectives for the treatment of cerebrovascular insufficiency related memory dysfunction.

Introduction

Cholinergic pathways have been shown to play an important role in the regulation of cerebral vascular resistance, relaxation and contraction of blood vessels, and regional blood flow [1–3]. It is well known that acetylcholine (Ach) is a powerful dilator of most vascular beds and that this activity is mediated by endothelial muscarinic Ach receptors triggering the release of the actual vasorelaxing agent, nitric oxide (NO) [4–8]. In a previous study, we demonstrated that M_5 receptors (M5R) mediate Ach-induced relaxation of cerebral but not of peripheral blood vessels [9], consistent with immunohistochemical [10] and pharmacological studies [11,12].

Ach binding to M5Rs leads to the activation of G proteins of the Gq family which in turns triggers increases in intracellular calcium and inositol 1,4,5-triphosphate levels [13–16] and eventually the activation of endothelial NO synthase (eNOS) and the production of NO [12]. Therefore, the constitutive constriction of cerebral arteries in male $M5R^{-/-}$ mice that we observed in a previous study [17] is most likely due to the lack of Ach-mediated NO release.

We previously reported that male M5R knockout ($M5R^{-/-}$) mice show a constitutive decrease in the diameter of the basilar artery and of middle cerebral arterioles, a reduction in cerebral blood flow (CBF), and impaired autoregulation of CBF, as compared to wildtype littermates [17]. Male $M5R^{-/-}$ mice also displayed dendritic atrophy in the cerebral cortex and hippocampus and impaired function of CA3 hippocampal pyramidal cells, probably secondary to cerebrovascular insufficiency [17]. Moreover, deficits in short-term memory (Y-maze) and cognitive

101

behavior (object recognition) were evident in male $M5R^{-/-}$ mice, consistent with impaired hippocampal function [17]. These data suggest that male $M5R^{-/-}$ mice are a suitable model for evaluating the effect of decreased CBF on neurologic function. Numerous animal models of chronic cerebral hypoperfusion have been generated by surgical methods. For example, one of these models showed white matter lesions, glial activation, and spatial memory deficits, mimicking several pathological aspects of human ischemia [18,19]. Male $M5R^{-/-}$ mice show also prolonged chronic cerebral hypoperfusion without necrosis in brain [17].

In the present study, we show that the phenotypic changes displayed by the male $M5R^{-/-}$ mice were absent in female $M5R^{-/-}$ mice. One possibility is that estrogens, the primary female sex hormones, protect female $M5R^{-/-}$ mice against the detrimental effects associated with the lack of M5Rs in males. Consistent with this notion, several studies have shown that estrogen increases CBF by stimulating the release of NO from vascular endothelial cells [20].

To test the hypothesis that estrogen protects against cerebrovascular and neuronal deficits caused by the absence of M5Rs, we conducted phenotyping studies with male $M5R^{-/-}$ mice bearing estrogen (E2) implants. We found that E2 treatment fully restored the diameter of the basilar artery to normal in male $M5R^{-/-}$ mice. Furthermore, treatment of male $M5R^{-/-}$ mice with estrogen also improved their cognitive performance in a Y-maze test and reduced the atrophy of neural dendrites in the cerebral cortex and hippocampus.

This study demonstrates that male $M5R^{-/-}$ mice, but not female $M5R^{-/-}$ mice, show a significantly increased number of GFAP positive cells in cortex and hippocampus, but the number of S100β positive astrocytes, a measure of the total number of astrocytes, remain unchanged. These astrocytic responses are unlikely associated with neural cells death or immunoglobulin *leakage* around cerebral blood vessels. This observation suggests that the lack of M5R in male mice leads to astrocytic swelling in cortex and hippocampus. Interestingly, E2 treatment of male $M5R^{-/-}$ mice completely restored normal GFAP expression levels in hippocampus. These findings indicate that $M5R^{-/-}$ mice represent an excellent novel model system to study the beneficial effects of estrogen on cerebrovascular function and cognition.

Results

### Gender difference of CBF in $M5R^{-/-}$ mice

We employed the Magnetic Resonance Angiography (MRA) based time-of flight (TOF) method to study the area of the basilar artery in male and female $M5R^{+/+}$ and $M5R^{-/-}$ mice. Ovariectomies were performed 4 month after birth using standard surgical procedures. To synchronize menstrual cycle length, we inject pregnant mare serum gonadotropin (PMSG) / human chorionic gonadotropin (hCG) into female mice by intraperitoneal injection (IP) before E2 treatment (see Material and Method section). MRA was carried out 2 week after ovariectomy (OVX) surgery and two days after PMSG/hCG treatments on 4 month-old female $M5R^{+/+}$ (n = 11) and $M5R^{-/-}$ mice (n = 12). TOF angiograms were obtained using a two-dimensional gradient-echo sequence (for additional experimental details, see Materials and methods). Three-dimensional angiograms of the MCA and the basilar artery (the segments indicated in **Figure 1A**) were obtained by using MATLAB software. Figure 1A shows that the diameter of the MCA and the basilar artery was similar in female $M5R^{+/+}$ and $M5R^{-/-}$ mice. In contrast, ovariectomized female $M5R^{-/-}$ mice showed a significant decrease in vascular diameter in the MCA and the basilar artery, as compared to intact female $M5R^{-/-}$ mice (**Figure 1A**).

For CBF measurements, we defined the branches of the MCA in the order from A1 to A3 (data not shown) and previously described in [17]. We measured the CBF of cerebral arterioles located on the cortical surface at the level of the peripheral branch of the MCA in male $M5R^{+/+}$ and $M5R^{-/-}$ mice (4-month-old) using laser-Doppler flowmeter. Under resting conditions, male $M5R^{-/-}$ mice showed a significantly lower ($p<0.001$) CBF than male $M5R^{+/+}$ mice at the A1 branch (see Supporting Information, **Figure S1**). However, female $M5R^{-/-}$ mice did not show any significant impairment in CBF, as compared to female $M5R^{+/+}$ mice (**Figure S1**). Furthermore, OVX $M5R^{-/-}$ mice showed impaired CBF ($p<0.001$), similar to male $M5R^{-/-}$ mice (**Figure S1**), suggesting that female sex hormones, such as estrogen, may be able to compensate for the impairment of cerebrovascular function caused by the lack of M5Rs in male mice.

Neuroanatomical and cognitive phenotypes of female and OVX female $M5R^{-/-}$ mice

Male $M5R^{-/-}$ mice showed a significantly reduced number of dendritic spines in cortical and hippocampal CA3 pyramidal neurons [17]. We therefore also examined the number of dendritic spines in cortical pyramidal neurons (layer V) from female $M5R^{+/+}$ and $M5R^{-/-}$ mice. Golgi staining studies revealed that cortical pyramidal neurons from female $M5R^{-/-}$ mice (4-month-old) showed no clear signs of atrophy of the basal-dendritic tree and apical dendrites (**Figure 1B**). However, OVX female $M5R^{-/-}$ mice (4-month-old) showed a similar phenotype as male $M5R^{-/-}$ mice (**Figure 1B**). Immunostaining experiments were carried out 2 weeks after OVX surgery and two days after PMSG/hCG treatment on 4 month-old females. The number of spines in basal dendrites was significantly reduced in OVX female $M5R^{-/-}$ mice, as compared with OVX female $M5R^{+/+}$ mice (**Figure 1B**) (number of spines per 10 μm length of dendritic segment: OVX female $M5R^{+/+}$ mice, 24.4±0.3; OVX female $M5R^{-/-}$ mice, 18.1±0.9; means±SEM; P<0.05; n = 40 dendritic segments from 3 animals per group). We also analyzed the expression of several key neuronal receptor proteins by using western blot analysis (cerebral cortex and hippocampus). Specifically, we examined the expression levels of the NR1 [N-methyl-D-aspartate (NMDA) receptor subunit], GluR1 (AMPA receptor subunit), and GluR5 (kainate receptor subunit) glutamate receptor subunits. We did not observe any significant differences in glutamate receptor expression levels between female $M5R^{-/-}$ and $M5R^{+/+}$ mice (4-month-old) (**Figure S2**). However, OVX female $M5R^{+/+}$ mice (4-month-old) showed significantly reduced expression levels of NR1 and GluR5 receptors in cortex and hippocampus ($p<0.05$; **Figure S2**) and reduced expression of GluR1 in cortex, as compared to OVX female $M5R^{+/+}$ mice. GluR1 expression levels in hippocampus remained unaffected (**Figure S2**).

We next examined short time memory in female $M5R^{-/-}$ and $M5R^{+/+}$ mice, using the Y-maze spontaneous alternation task [17]. We found that locomotor activity did not differ significantly between the four groups (female $M5R^{+/+}$ mice, female $M5R^{-/-}$ mice, OVX female $M5R^{+/+}$ mice, OVX female $M5R^{-/-}$ mice; data not shown). The Y-maze test was carried out 2 weeks after OVX surgery and two days after PMSG/hCG treatment on 4 month-old females. In the Y-maze task, female $M5R^{-/-}$ mice (4-month-old) showed no significant impairments in spatial memory (**Figure 1C**). However, OVX female $M5R^{-/-}$ mice (4-month-old) showed impaired spontaneous alternation performance, similar to the male $M5R^{-/-}$ mice [17] ($p<0.05$; **Figure 1C**).
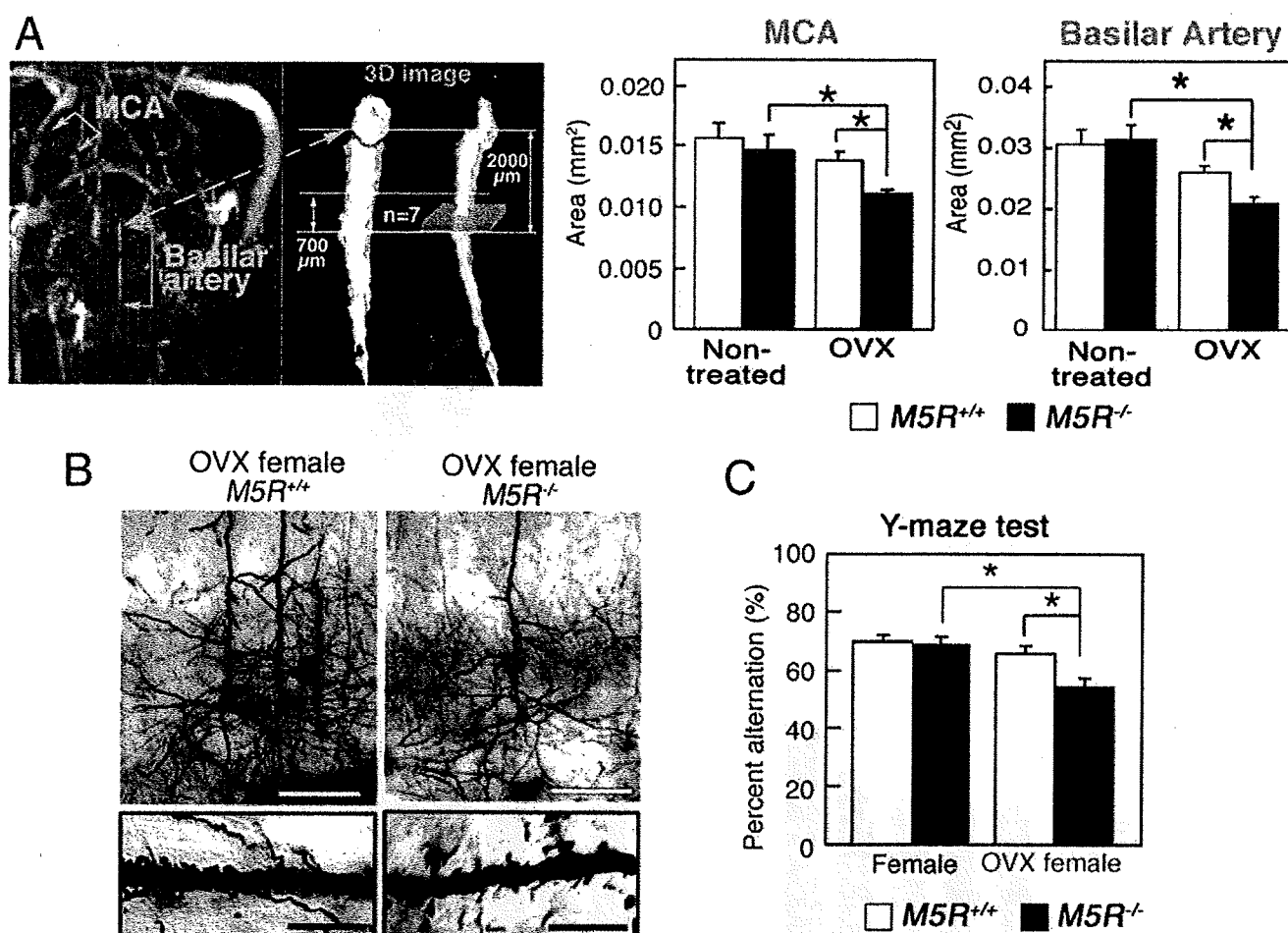
Figure 1. Gender-specific phenotypic differences displayed by *M5R*$^{-/-}$ **mice.** (A) First, rapid scanning for the basilar artery provide the each portion of artery (left image; 3D angiograms of the basilar artery from female *M5R*$^{+/+}$ mice). Second, the vascular area of each portion of the basilar artery was measured by the high resolution imaging within 30 min on a perpendicular section of the vessel (the site where the basilar artery enters the circle of Wills), and mean vascular area was determined as the average of the 7 segments on the measured area of each 100 μm intervals (right image). Ovariectomies were performed 4 months after birth using standard surgical procedures. To synchronize menstrual cycle length, we injected pregnant mare serum gonadotropin (PMSG)/human chorionic gonadotropin (hCG) into female mice by IP injection before E2 treatment (see Materials and Methods section). MRA was carried out 2 weeks after OVX surgery and two days after PMSG/hCG treatment on 4 month-old female *M5R*$^{+/+}$ (n = 11) and *M5R*$^{-/-}$ (n = 12) mice. Values are means±SE. *$p<0.05$. (B) Morphologic changes of cortical pyramidal neurons (layer V) from OVX female *M5R*$^{-/-}$ mice. Golgi staining studies revealed that cortical pyramidal neurons from OVX female *M5R*$^{-/-}$ mice showed clear signs of atrophy of the basal-dendritic tree and apical dendrites. White scale bars in upper panels, 50 μm; black scale bars in lower panels, 10 μm. (C) Performance of female *M5R*$^{-/-}$ and *M5R*$^{+/+}$ mice, as well as OVX *M5R*$^{-/-}$ and OVX *M5R*$^{+/+}$ mice, in the Y-maze spontaneous alternation task. Note that only OVX female *M5R*$^{-/-}$ mice showed a performance deficit in this test. Data are given as means±SEM; female *M5R*$^{+/+}$, n = 11 mice; female *M5R*$^{-/-}$, n = 12 mice OVX female *M5R*$^{+/+}$, n = 20 mice; OVX female *M5R*$^{-/-}$, n = 20 mice; *$p<0.05$.
doi:10.1371/journal.pone.0005159.g001

Mitogen-activated protein kinase (MAPK) activation and NO release by a muscarinic agonist and E2 in TM-BBB cells

17β-estradiol (E2), the primary estrogen, has been reported to signal rapidly through ERK/MAP kinase [21–23] and PI3K/Akt [20,24] to induce eNOS activity and NO generation in peripheral blood vessel derived cells [25,26] and in neuroblastoma cells [27]. To examine the effect of estrogen on NO release in cerebral endothelial cells, we used the immortalized TM-BBB cell line, which is derived from mouse brain vascular endothelial cells [28] (See material and methods). TM-BBB cells were treated with bethanechol (Bch; 100 μM), a muscarinic receptor agonist, and E2 (10 nM) for 0–60 min. Bch and E2 induced the phosphorylation of ERK1/2 in a similar manner (**Figure 2A,B**). Moreover, both compounds stimulated NO production by ∼1.6-fold at the

180 min time point (**Figure 2B**). These results support the concept that both muscarinic and estrogen receptor signaling leads to enhanced NO production via activation of eNOS through ERK 1/2 pathways in TM-BBB cells [29–31].

RT-PCR studies showed that TM-BBB cells express M5Rs but not M3Rs which are normally found on non-cerebral arteries [32,33], as well as ERα, ERβ and GPR30 estrogen receptors (**Figure 3A**) (See material and methods). Therefore, we also treated TM-BBB cells with selective estrogen receptor agonists, ERα (1,3,5-Tris(4-hydroxyphenyl)-4-propyl-1H-pyrazole (10 μM PPT), ERβ (10 μM DPN), and GPR30 (10 μM G1) for 60 min. Subsequently, cell lysates were prepared and analyzed by western blotting with anti-pERK or anti-total ERK antibodies. This analysis revealed the increased ERK1/2 phosphorylation mediated by 10 μM PPT, 10 μM DPN, or 10 μM G1 for 60 min (**Figure 3B**).
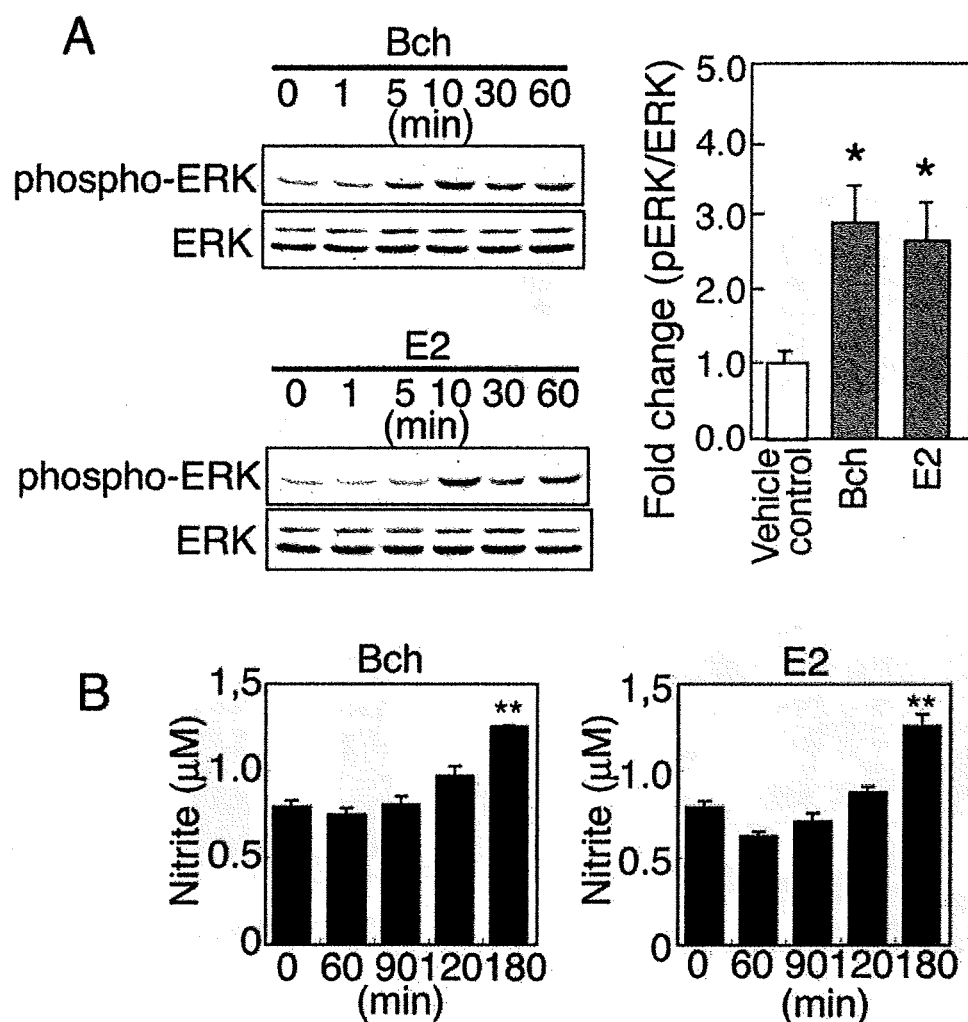
Figure 2. Bethanechol and E2 induce ERK phosphorylation and NO production in TM-BBB cells in a time-dependent manner. (A) TM-BBB cells were stimulated with 100 μM of the muscarinic agonist, bethanechol (Bch), or 10 nM E2 for different periods of time (1–60 min), and cell lysates were analyzed by western blotting with anti-pERK or anti-total ERK antibodies. The cumulative results of Western blot analysis are reported from three independent experiments (10 min after treatment with Bch or E2). Values are means±SEM. *$p<0.05$ (vs vehicle control). (B) TM-BBB cells were stimulated with 100 μM Bch or 10 nM E2 for different time periods. Subsequently, nitrite levels were measured in the culture medium. Values are means±SEM. **$p<0.001$ (vs vehicle control).
doi:10.1371/journal.pone.0005159.g002

Restoration of normal cerebral artery diameter by E2 in male $M5R^{-/-}$ and OVX female $M5R^{-/-}$ mice

MRA experiments were carried out 2 weeks after OVX surgery and two days after PMSG/hCG treatment on 4 month-old females. **Figure 4B** shows that the diameter of the basilar artery was similar in female $M5R^{+/+}$ and $M5R^{-/-}$ mice (schematic representation of the E2 injection and MRA monitoring schedule, see **Figure 4A**). In contrast, OVX female $M5R^{-/-}$ mice showed a significant decrease in vascular diameter, as compared to intact female $M5R^{-/-}$ mice (**Figure 4B**). Moreover, treatment of OVX female $M5R^{-/-}$ mice with E2 (1 μg E2 was injected into the tail vein) completely prevented these deficits (**Figure 3B**). We noted that PMSG/hCG treatment did not significantly affect the diameter of the basilar artery in female mice (**Figure 4B**) and E2-treated male mice (**Figure S3B**).

As reported previously [17], the diameter of the basilar artery was significantly reduced in male $M5R^{-/-}$ mice, as compared to male $M5R^{+/+}$ mice (**Figure 4C**). Strikingly, E2 treatment (1 μg E2

was injected into the tail vein) of male $M5R^{-/-}$ mice led to an increase in the diameter of the basilar artery, similar to that observed with control male $M5R^{+/+}$ mice (**Figure 4C**). On the other hand, in male $M5R^{+/+}$ mice, E2 injection had no significant effect on vascular diameter (**Figure 4C**).

Normalization of neurite atrophy and cognitive function by E2 treatment of male $M5R^{-/-}$ mice

We next examined whether the deficits displayed by male $M5R^{-/-}$ mice could be overcome by chronic (3 weeks) E2 treatment (an 0.1 mg E2 pellet was implanted in the neck). As expected [34], non-treated male $M5R^{-/-}$ mice (4 months old mice) showed a significant decrease in the diameter of the basilar artery (**Figure 5B**) (a schematic representation schedule of E2 tablet implantation and MRA monitoring is given in **Figure 5A**). Strikingly, E2 treatment of male $M5R^{-/-}$ mice led to a recovery of vascular diameter, similar to that of control male $M5R^{+/+}$ mice (**Figure 5B**). PMSG/hCG treatment had not significant effect on

104
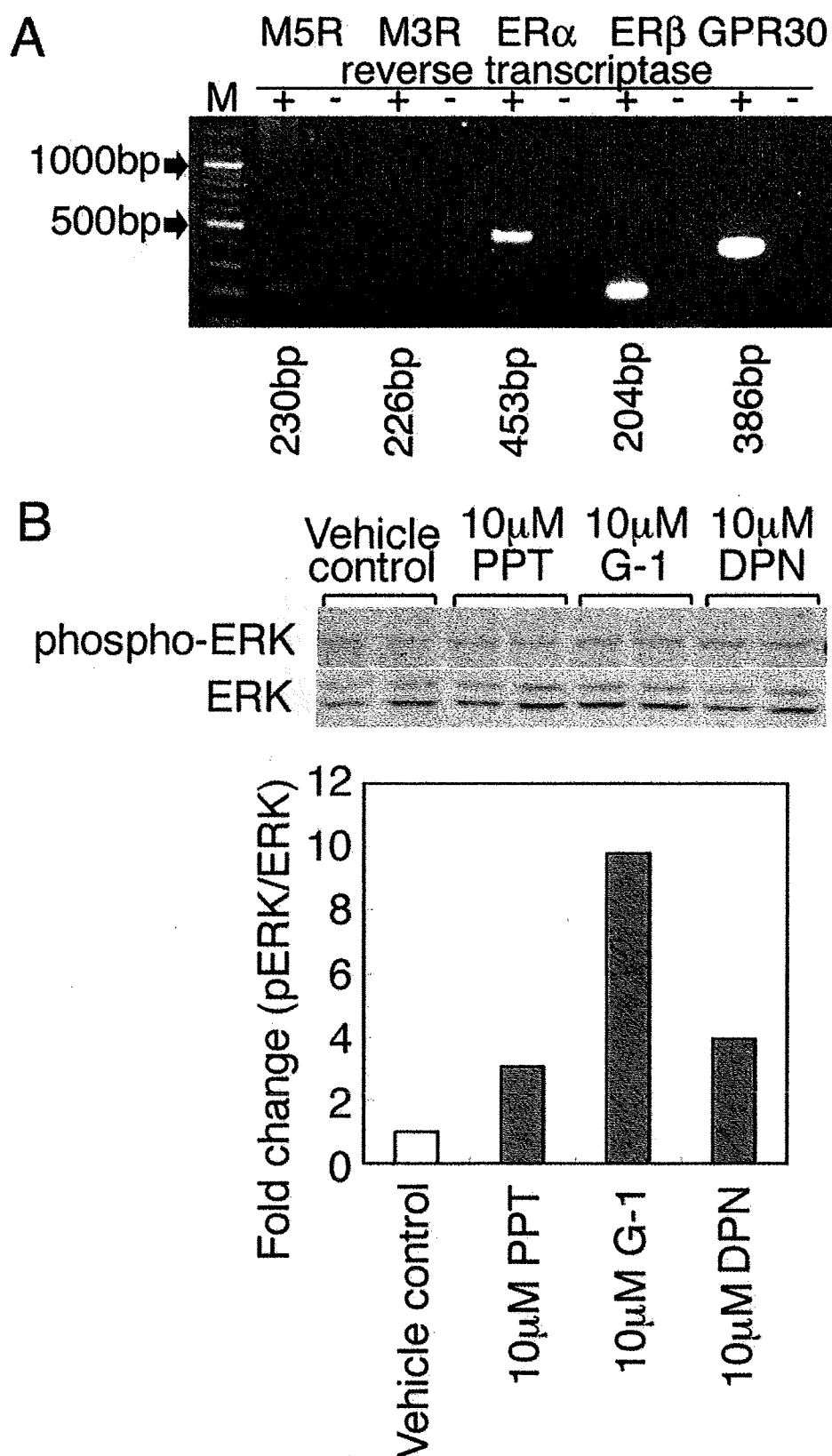
Figure 3. Agonists of ERα, ERβ, and GPR30 promoted ERK activation in TM-BBB cells. (A) RT-PCR analysis demonstrating the presence of transcripts of M3 muscarinic receptor (226 bp), M5 muscarinic receptor (230 bp), ERα estrogen receptor (453 bp), ERβ estrogen receptor (204 bp) and GPR30 estrogen receptor (386 bp) in TM-BBB cells. (B) TM-BBB cells were stimulated with the estrogen receptor agonists, PPT (ERα), DPN (ERβ), or G1 (GPR30) for 60 min, and cell lysates were analyzed by western blotting with anti-pERK or anti-total ERK antibodies.
doi:10.1371/journal.pone.0005159.g003

A

Non-surgery female mice
or
OVX female mice

PMSG/hCG
IP injection

Male

MRA Prior to
E2 treatment

Basilar artery

E2 injection into the tail vein

MRA

Basilar artery

Measuring by high resolution
imaging within 30 min

B

Female mice   Basilar artery

Area (mm²)

□ M5R⁺/⁺
▦ M5R⁻/⁻

Non-surgery Female mice   OVX Female mice

PMSG/hCG	-	-	+	+	-	-	+	+	-	-	+	+	-	-	+	+
E2 treatment	-	+	-	+	-	+	-	+	-	+	-	+	-	+	-	+

C

Male
Basilar artery

Area (mm²)

□ M5R⁺/⁺
■ M5R⁻/⁻

Prior to   E2
treatment treatment

Figure 4. E2 injection completely restores the cross-sectional area of the basilar artery in male $M5R^{-/-}$ mice as well as in OVX female $M5R^{-/-}$ mice. (A) Schematic representation of the E2 injection and MRA monitoring schedule used. (B) Vascular area of the basilar artery in female $M5R^{+/+}$, $M5R^{-/-}$, OVX $M5R^{+/+}$, OVX $M5R^{-/-}$, and E2 injected OVX $M5R^{+/+}$and $M5R^{-/-}$ mice. MRA was carried out 2 week after OVX surgery on 4 month-old female $M5R^{+/+}$ (n = 15) and $M5R^{-/-}$ (n = 15) mice. MRA was carried out 2 week after OVX surgery and two days after PMSG/hCG treatment on 4 month-old female $M5R^{+/+}$ (n = 14) and $M5R^{-/-}$ (n = 14) mice. After MRA analysis, 1 μg E2 was injected into the tail vein, followed by MRA 30 min after injection. Values are means±SE. **$p<0.001$. (C) Vascular area of the basilar artery in male $M5R^{+/+}$and $M5R^{-/-}$ mice and E2 injected male $M5R^{+/+}$ and $M5R^{-/-}$ mice. 3.5–4.5 month-old male $M5R^{+/+}$ (n = 6) and $M5R^{-/-}$ (n = 10) mice were used for MRA analysis and 1 μg E2 was injected into the tail vein, followed by MRA 30 min after injection. Values are means±SEM. **$p<0.001$.
doi:10.1371/journal.pone.0005159.g004

the diameter of the basilar artery in male mice during transient or chronic E2 treatment experiments (**Figure S3**).

Hypoxic conditions affect the pH of cerebral blood serum. However, the collection of cerebral blood serum for pH measurements is technically very difficult in mice. The Na^+/H^+ exchanger isoform 1 (NHE1) is known to be essential for the maintenance and regulation of pH in cortical astrocytes [35]. NHE1 is also known to slightly detectable in cortical neurons [35]. We therefore examined NHE1 expression levels in astrocytes of fimbria hippocampus, an area enriched with GFAP positive astrocytes. If reduced CBF causes acidosis associated with hypoxia in the brain of male $M5R^{-/-}$ mice, NHE1 is predicted to be upregulated in cortical astrocytes [36]. We demonstrated that NHE1 immunolabeling was abundantly associated with plasma membrane structures of choroid plexus between fimbria of hippocampus and cortex (**Figure 5C**). In male $M5R^{-/-}$ mice, the intensity of NHE1 immunostaining was markedly increased in GFAP positive astrocytes in fimbria hippocampus (**Figure 5C**). E2 treatment of male $M5R^{-/-}$ mice restored normal NHE1 immunostaining, similar to that of control male $M5R^{+/+}$ mice (**Figure 5C**).

Normalization of astrocytic swelling in cortex and hippocampus by E2 treatment of male $M5R^{-/-}$ mice

Under hypoxic conditions, changes in estrogen levels can lead to astrocytic swelling in the brain [37,38]. On the basis of these findings, we studied the number and morphology of astrocytes in the cortex and hippocampus of E2 treated male $M5R^{-/-}$ and $M5R^{+/+}$ mice, as well as non-treated male $M5R^{-/-}$ and $M5R^{+/+}$ mice. We found that non-treated male $M5R^{-/-}$ mice showed a significant increase in the number of GFAP positive cells in cortex (**Figure 4A**) and hippocampus (**Figure 4A, Figure S4A–C**), but the number of S100β positive astrocytes, a measure of the total number of astrocytes, remained unchanged. Furthermore, GFAP positive astrocytes in non-treated male $M5R^{-/-}$ mice showed many astrocytic processes (**Figure S4C**). However, male $M5R^{-/-}$ mice did not show migration of microglia (Iba-1 or Mac-2 positive cells) in cortex and hippocampus (**Figure S4C**). To examine the intactness of the blood brain barrier (BBB), we injected 25 mg/kg Evans blue (EB) into the tail vain of 6-month-old male $M5R^{-/-}$ and $M5R^{+/+}$ mice, followed by visualization of auto-fluorescence of EB in cortical tissue [39]. Since EB binds to albumin, red fluorescence of EB observed in tissue indicates leakage of blood

106
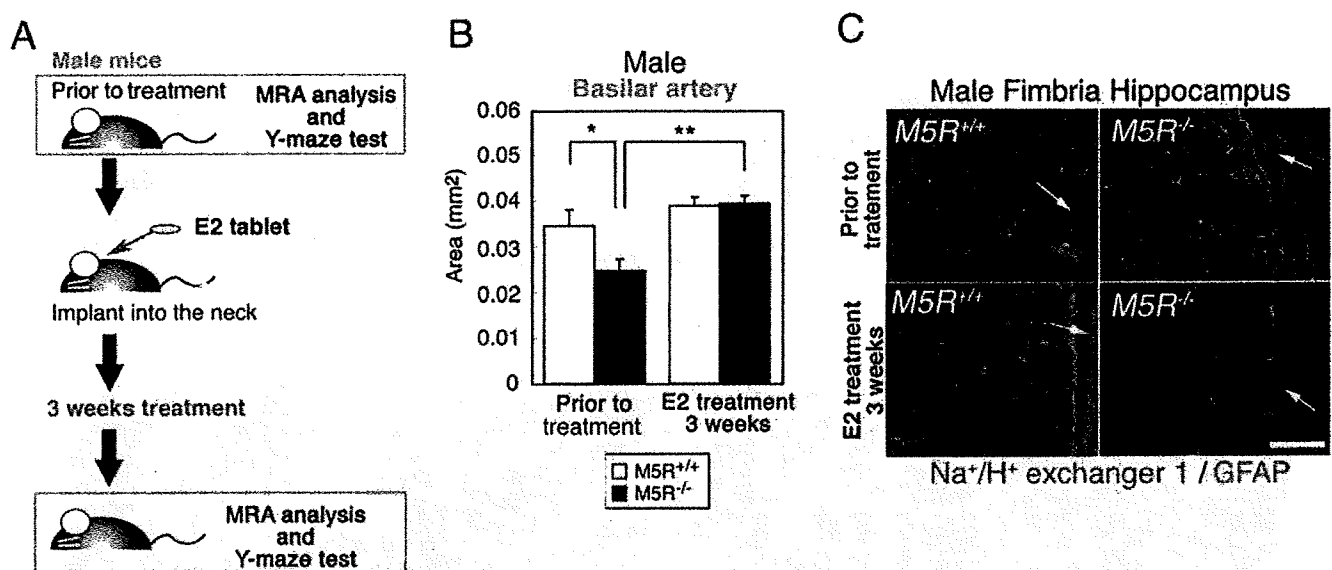
Figure 5. Chronic E2 treatment rescues cerebrovascular deficits in male $M5R^{-/-}$ mice. (A) A schematic representation schedule of E2 tablet implantation and MRA monitoring. (B) Chronic E2 treatment completely rescues cerebrovascular deficits in 3.5 month-old male $M5R^{-/-}$ mice. After MRA, an E2 tablet (0.1 mg / 21 days release) was implanted into the neck of each mouse, followed by MRA testing 3 weeks after the start of E2 administration. (C) The increased NHE1 expression levels in male $M5R^{-/-}$ mice. Na^+/H^+ exchanger isoform 1 (NHE1)is indicated by Red color. The GFAP is indicated by Green color. The site where the choroid plexus between fimbria of hippocampus and ventricle is indicated by arrows. Scale bar; 100 μm.

doi:10.1371/journal.pone.0005159.g005

vessels. Leakage of EB in surrounding blood vessels was not detected in cortex and hippocampus of male $M5R^{-/-}$ and $M5R^{+/+}$ mice (**Figure S4E**). These data suggest that astrocytic swelling in male $M5R^{-/-}$ brain is unlikely to be associated with inflammation around cortical or hippocampal blood vessels. Moreover, non-treated female $M5R^{-/-}$ mice did not show a significant increase in the number of GFAP positive cells in cortex and hippocampus compared to female $M5R^{+/+}$ mice (4 months old; **Figure 6A**). However, 4-month-old OVX female $M5R^{-/-}$ mice showed activated GFAP positive astrocytes in cortex and hippocampus (**Figure 6A**), similar to male $M5R^{-/-}$ mice (**Figure 6B, Figure S4A–C**) (morphological analysis was carried out 2 weeks after OVX surgery on 4 month-old female $M5R^{+/+}$ and $M5R^{-/-}$ mice), suggesting that female sex hormones, such as estrogen, may be able to compensate for the astrocyte activation caused by the impairment of cerebrovascular function. Strikingly, E2 treatment (an 0.1 mg E2 pellet was implanted in the neck) of male $M5R^{-/-}$ mice restored normal GFAP expression levels (**Figure 6B, Figure S4B**). On the other hand, E2-treated male $M5R^{+/+}$ control mice showed similar levels of GFAP expression in cortex and hippocampus as non-treated $M5R^{+/+}$ mice (**Figure 6B, Figure S4A,B**).

To exclude the possibility that E2 treatment upregulates GFAP gene expression levels in male $M5R^{-/-}$ mice, we carried out morphological studies on CA3 hippocampal astrocytes using three-dimensional reconstruction of electron microscope images (**Figure 6C**). A total of 100–110 sections of 70 nm electron microscope images were reconstructed to visualize astrocyte shapes (see three-dimensional reconstruction of electron microscope images in Supplemental movies; non-treated male $M5R^{+/+}$ mice, **Movie S1**; non-treated male $M5R^{-/-}$ mice, **Movie S2**; E2-treated male $M5R^{+/+}$ mice, **Movie S3**; E2-treated male $M5R^{-/-}$ mice **Movie S4**). This analysis showed that the astrocyte activation leaded to the swollen astrocyte foot processes in male $M5R^{-/-}$ mice were markedly reduced in E2-treated male $M5R^{-/-}$

mice (**Figure 6C**). It is therefore unlikely that E2 treatment leads to changes in *gfap* gene expression levels in male $M5R^{-/-}$ mice.

Normalization of neural morphology in cortex and hippocampus by E2 treatment of male $M5R^{-/-}$ mice

We examined the effect of chronic (3 weeks) E2 treatment on astrocyte morphological changes. As expected, non-treated male $M5R^{-/-}$ mice (4 months old) showed a significant reduction in spine number in cortical (**Figure 7A,B**) and CA3 hippocampal pyramidal neurons (**Figure 7C**), and synapse number in CA3 hippocampal pyramidal neurons (**Figure 7D**). However, after 3 weeks of E2 treatment, these morphological deficits were greatly ameliorated (**Figure 7A–D**).

We also examined the effect of chronic E2 treatment on the performance of male $M5R^{-/-}$ and $M5R^{+/+}$ mice in the Y-maze spontaneous alternation test which is commonly employed to assess spatial working memory. As reported previously, male $M5R^{-/-}$ mice (4 months old) showed pronounced deficits in spontaneous alternation performance ($p<0.05$; **Figure 7D**), as compared to male $M5R^{+/+}$ mice. After chronic E2 treatment, male $M5R^{-/-}$ mice did no longer show any significant impairments in this task (**Figure 7D**), indicating that E2 enhances cognitive function in male $M5R^{-/-}$ mice.

Discussion

The therapeutic utility of estrogen in postischemic treatment paradigms has been studied using chronic cerebral hypoperfusion models. E2 administered after permanent middle cerebral artery occlusion or reversible middle cerebral artery occlusion reduces infarction size in ovariectomized female rats [40–42]. In these studies, estrogen is thought to act as a cerebral vasodilator and to protect vascular integrity. However, surgically induced animal models of cerebral hypoperfusion also lead to neuronal death and
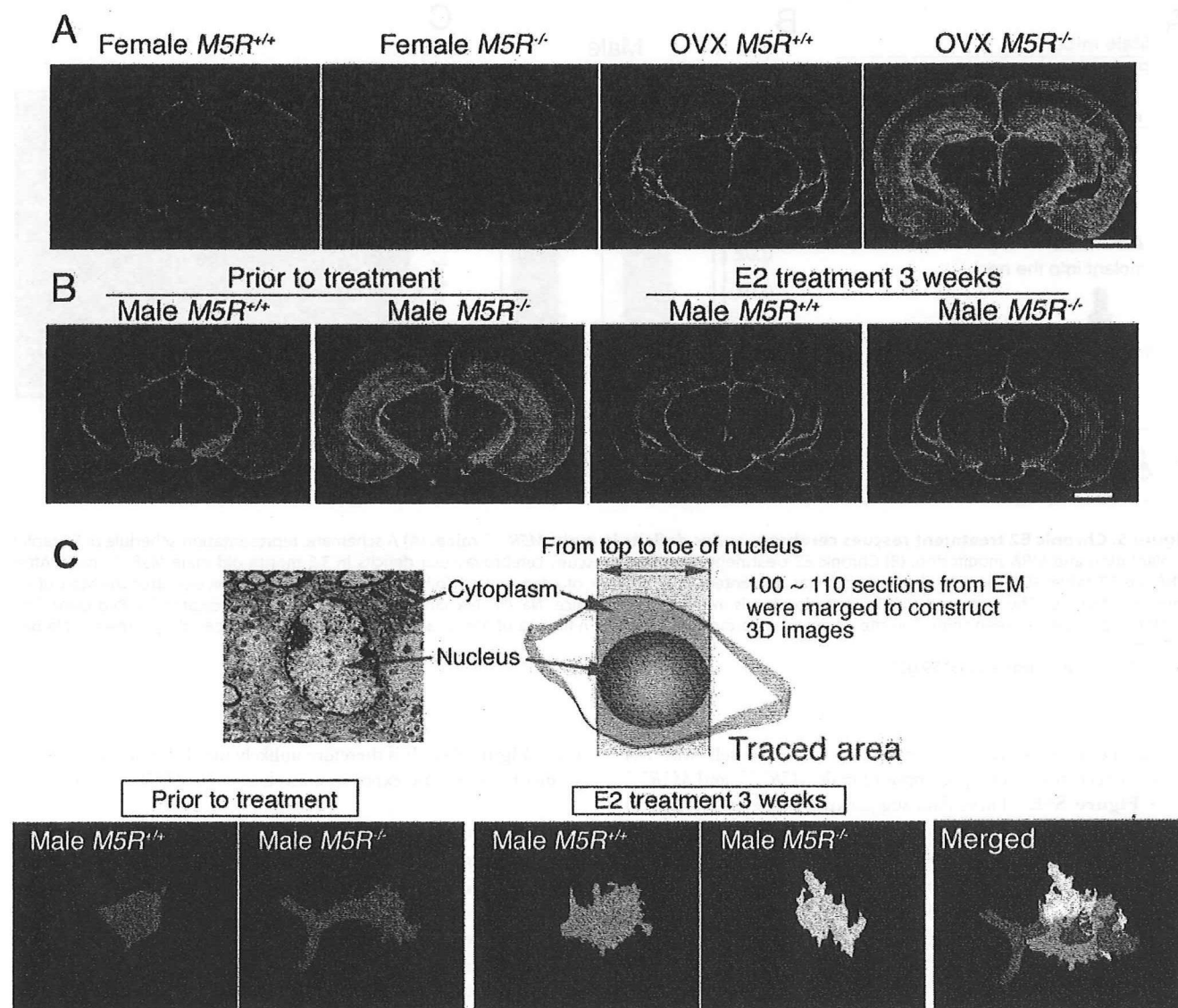
Figure 6. Male $M5R^{-/-}$ mice exhibit astrocyte swelling which is rescued by E2 treatment. (A) Female $M5R^{-/-}$ mice exhibit GFAP immunoreactivity similar to female $M5R^{+/+}$ mice in the cortex and the CA3 region of hippocampus. Immunostaining experiments were carried out 2 weeks after OVX surgery and two days after PMSG/hCG treatment on 4 month-old females. OVX $M5R^{-/-}$ female mice showed a significantly increased immunoreactivity of GFAP positive cells. Scale bar = 1 mm. (B) GFAP immunostaining shows astrocyte activation in cortex and hippocampus in 4-month-old male $M5R^{-/-}$ mice. However, E2 treatment of male $M5R^{-/-}$ mice restored normal GFAP expression levels. Frozen sections of the brain (coronal section) were prepared from male $M5R^{-/-}$ and $M5R^{+/+}$ mice without or after chronic E2 treatment (3 weeks, 1 µg E2 was injected into the tail vein). For details, see the legend to Fig. 3D. Scale bar = 1 mm. (C) Astrocytic swelling in the CA3 hippocampal astrocytes was visualized using three-dimensional reconstruction of electron microscope images. A total of 100–110 sections of 70 nm electron microscope images were reconstructed to visualize astrocytic shapes.
doi:10.1371/journal.pone.0005159.g006

inflammation [18,19]. It is therefore possible that the E2-mediated reduction of infarction size seen in these models may be caused by anti-inflammatory or anti-apoptotic activities of E2 [43,44]. Thus, $M5R^{-/-}$ mice represent a novel genetic model of chronic cerebral hypoperfusion that can provide new insight into beneficial effects of estrogen in the absence of necrotic or inflammatory processes.

We demonstrated that male $M5R^{-/-}$ mice displayed a significantly increased immunostaining of GFAP positive cells in cortex and hippocampus, indicative of astrocytic activation. One possibility is that this defect is responsible for the dendritic atrophy and loss of neural functions in these regions displayed by male $M5R^{-/-}$ mice. These findings suggest that male $M5R^{-/-}$ mice

represent a novel model to study the physiological and pathophysiological roles of the central cholinergic vasodilator system in regulating CBF, reactive astrocytic swelling and cognitive processes.

Strikingly, the phenotypic changes displayed by male $M5R^{-/-}$ mice were not observed in female $M5R^{-/-}$ mice, suggesting that female sex hormones might modulate CBF in female $M5R^{-/-}$ mice. Consistent with this notion, we observed that estrogen (E2) was able to release NO from cerebral vascular endothelial cells (NO is predicted to trigger vasodilation and increase CBF).

To test the hypothesis that estrogen may rescue the phenotypic deficits displayed by male $M5R^{-/-}$ mice, we implanted estrogen

108
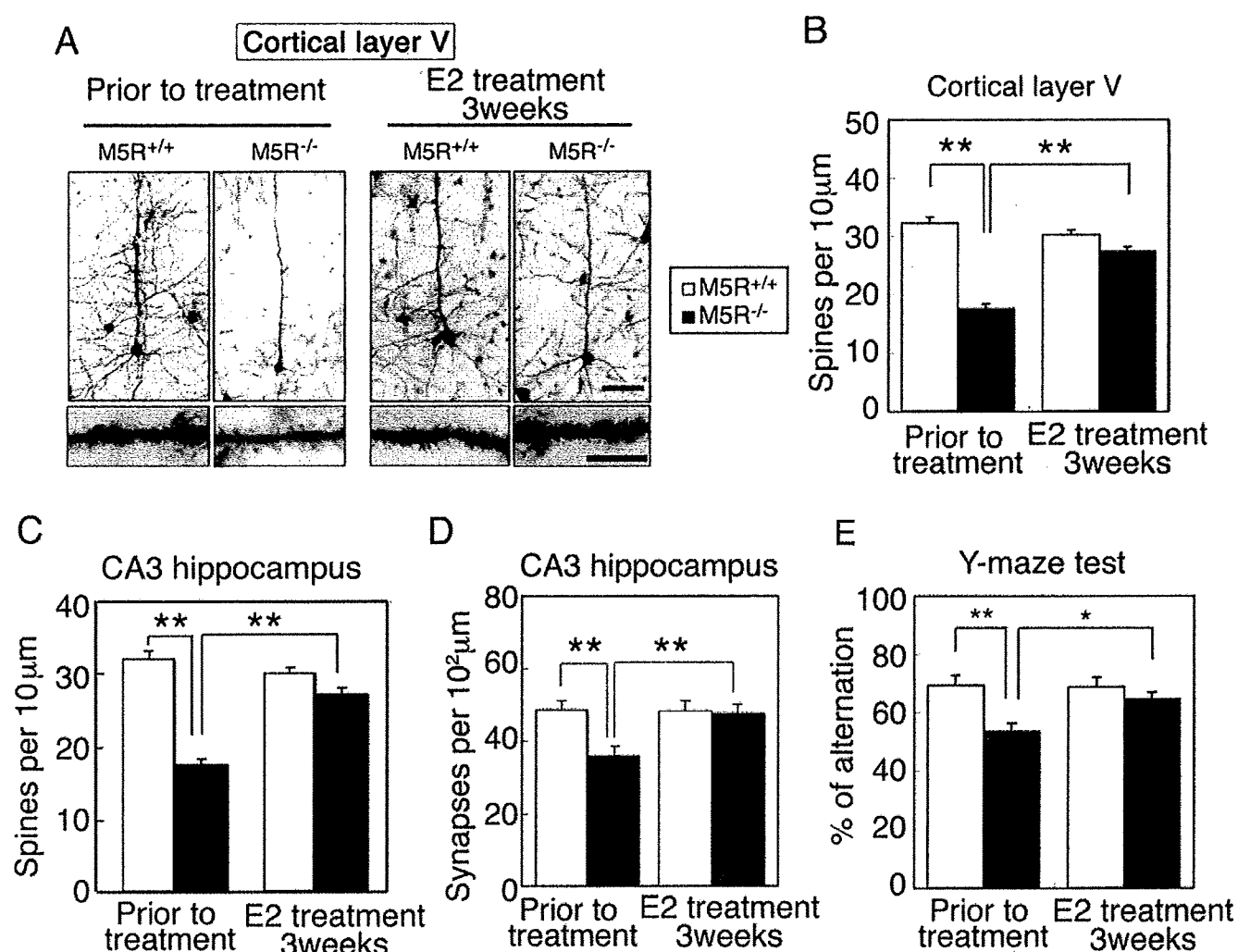
Figure 7. E2 restores normal morphology in cortical and hippocampal pyramidal neurons from male _M5R_^{−/−} mice. (A) Morphologic changes of cortical pyramidal neurons (layer V) from male _M5R_^{−/−} mice without or after chronic E2 treatment (3 weeks). Golgi staining revealed that cortical pyramidal neurons from male _M5R_^{−/−} mice showed clear signs of atrophy of the basal-dendritic tree and apical dendrites. E2 treated male _M5R_^{−/−} mice showed a similar morphology of spines in the basal-dendritic tree and apical dendrites as _M5R_^{+/+} control mice. (B) Number of spines per 10 μm length of dendritic segment of cortical pyramidal neurons (layer V) from male _M5R_^{−/−} and _M5R_^{+/+} mice, and E2 treated male _M5R_^{−/−} and _M5R_^{+/+} mice. N = 40 dendritic segments from 5 animals per group. (C) Number of spines per 10 μm length of dendritic segment of CA3 hippocampal pyramidal neurons from male _M5R_^{−/−} and _M5R_^{+/+} mice, and E2 treated male _M5R_^{−/−} and _M5R_^{+/+} mice. Hippocampal neurons from male _M5R_^{−/−} mice exhibited a significantly reduced number of dendritic spines. E2 administration also restored the number of dendritic spines in the CA3 hippocampus. N = 20 dendritic segments from 5 animals per group. Values are means±SEM. **$p<0.001$. (D) The number of synapses per 10^2 μm was counted in the CA3 hippocampus by analyzing electron microscope images. A total of 100–110 sections of 70 nm electron microscope images were counted for each sample. Values are means±SEM. **$p<0.001$. (E) Performance of male _M5R_^{+/+} and _M5R_^{−/−} mice prior to and after chronic E2 treatment in a Y-maze spatial-memory test. Chronic E2 tablet (0.1 mg / 21 days release) treatment completely rescues cerebrovascular and cognitive deficits in male _M5R_^{−/−} mice. All studies were carried out with 3 month-old male _M5R_^{+/+} (n = 16) and _M5R_^{−/−} (n = 14) mice. Values are means±SEM. *$p<0.05$, **$p<0.001$.
doi:10.1371/journal.pone.0005159.g007

pellets in the dorsum of male _M5R_^{−/−} mice, and initially performed MRA measurements on the basilar artery three weeks post-implantation. We found that the diameter of the basilar artery was restored to normal in male _M5R_^{−/−} mice treated with estrogen. Several studies have shown that M5Rs are expressed by cerebral endothelial cells [9,10]. Estrogen receptors (ERs) have also been shown to be expressed by vascular endothelial and smooth muscle cells [45,46]. Estrogen binding to membrane-bound ERs can lead to the activation of G proteins such as Gs and Gq [47,48]. M5Rs and ERs may therefore be linked to common signaling pathways in cerebral endothelial cells. The observed rapid activation of MAPKs by E2 in TM-BBB cells may therefore

reflect the activation of membrane-bound ERs linked to G protein signaling pathways. Consistent with this concept, the novel membrane estrogen receptor GPR30 [29–31] was also detected in the TM-BBB cell line (**Figure 3A**). We found that PPT (an ERα agonist), DPN (an ERβ agonist), and G1 (a GPR30 agonist) promoted ERK activation (**Figure 3B**). Therefore, a combination of estrogen receptors, ERα, ERβ, and GPR30, may allow for sufficient ERK1/2 phosphorylation.

E2-mediated NO production has been linked to vasodilation and is thought to involve stimulation of eNOS following rapid activation of phosphatidylinositol-3 kinase (PI3K)/Akt or MAPK signaling in different vascular tissues [20,21,25,49].

In the present study, we demonstrated that OVX female $M5R^{-/-}$ mice, in contrast to non-OVX female $M5R^{-/-}$ mice, suffer from a constitutive constriction of cerebral arteries, reduced CBF, dendritic atrophy (**Figure 1A**), and short-term memory loss (**Figure 1C**). We also found that E2 injection completely restored the diameter of the basilar artery in OVX female $M5R^{-/-}$ mice (as compared to non-OVX female $M5R^{-/-}$ mice). E2 partially restored the vascular area in OVX female $M5R^{+/+}$ mice (as compared to non-OVX female $M5R^{+/+}$ mice). In addition, E2 rescued the constitutive constriction of the basilar artery in male $M5R^{-/-}$ mice. These results suggest that estrogen (E2) can compensate for the lack of M5R-mediated vasodilation in cerebral blood vessels in $M5R^{-/-}$ mice. $M5R^{-/-}$ mice can therefore be used as novel model to examine the vasodilator effects of estrogen *in vivo*. Therefore, estrogen therapy may be clinically useful not only for female but also for male patients suffering from cerebrovascular deficits.

It is known that ischemia results in a marked reduction of tissue pH [50] and cerebral ischemia has been demonstrated to produce an intracellular acidosis in the ischemic core as well as in the ischemic penumbra [51]. For example, the NHE1 is one of the major acid extrusion mechanisms after intracellular acidosis. NHE1 catalyzes the electroneutral exchange of H^+ and Na^+ ions across cellular membranes, thereby regulating the pH of the cytoplasm [52,53]. Therefore, expression of NHE1 is thought to protect cells from internal acidification and to regulate cell volume in response to hypoxia. We found significantly increased NHE1 expression levels in male $M5R^{-/-}$ mice (**Figure 5C**). Swollen astrocyte foot processes lead to changes in brain extracellular space volume, composition, and geometry in aged animals with severe learning impairment [49]. It is hypothesized that the degree of hippocampal learning impairment in aged animals is related to astrocyte swelling [49]. Therefore we speculated that hypoxic stimulation induced astrocyte activation might contribute to the changes of neural activity in brain of male $M5R^{-/-}$ mice. We found that the lack of M5Rs in male mice was associated with cortical and hippocampal astrocytic swelling and deficits in dendritic morphology. It is well known that changes in astrocyte function regulate synaptic transmission [54–57]. It is tempting to speculate that the astrocytic swelling phenotype observed with male $M5R^{-/-}$ mice is a consequence of cerebrovascular insufficiency. Strikingly, E2 treatment of male $M5R^{-/-}$ mice led to a reversal of the astrocytic swelling phenotype, which can occupy extra-synaptic spaces (**Figure 6C**), and restored normal numbers of dendritic spines of pyramidal neurons in cortical and hippocampal pyramidal neurons (**Figure 7A–D**). Treatment with E2 also improved the performance of male $M5R^{-/-}$ mice in a cognitive test (Y-maze spontaneous alternation task)(**Figure 7E**). Estrogen treatment did not affect GFAP expression levels in male $M5R^{+/+}$ mice, as studied by western blotting analysis (**Figure S4B**). It is therefore unlikely that E2 acts on astrocytes directly to reduce GFAP immunoreactivity. GFAP expression levels were strikingly correlated with NHE1 expression levels in astrocytes, probably as a consequence of the hypoxic state of the brain of male $M5R^{-/-}$ mice. Our findings support the idea that E2 regulates important neuroprotective mechanisms *in vivo* by acting directly on endothelial cells and/or through glial cell intermediaries. Estrogen has been demonstrated to have numerous effects on glial cells and neurons. Besides affecting CBF by acting on vascular ERs, E2 may protect against neuronal damage through actions on glial cell activation [36,37]. Furthermore, animal studies suggest that E2 has neuroprotective effects against excitotoxicity [58], oxidative damage [59], and cerebral ischemia [60]. Our observations support the concept that the beneficial effects of estrogen on neural function observed in the present study are due to cerebral vasodilation controlling astrocyte activation as well as a direct neuroprotective effect. Clearly, additional studies are needed to examine the causal relationship between the cerebrovascular, neuromorphological, and behavioral deficits displayed by male $M5R^{-/-}$ mice and to further explore the mechanisms underlying the ability of estrogen to reverse these phenotypes.

Materials and Methods

Animals

$M5R^{-/-}$ mice were produced as described previously [9]. The average menstrual cycle length is 4 days in mice. To synchronize menstrual cycle length, we injected pregnant mare serum gonadotropin (PMSG)/human chorionic gonadotropin (hCG) into female mice by intraperitoneal (IP) injection before E2 treatment. Female mice were primed with an IP injection of 7.5 IU of PMSG and 7.5 IU of hCG to induce ovulation. After two days, female mice were subjected to the experiments. Animal experiments were approved by the Animal Experiment Committee of the RIKEN Brain Science Institute.

Measurement of CBF using a laser Doppler flowmeter

CBF measurements were performed as previously described [17]. The branches of the MCA were defined in the order from A1 to A3 [17]. A probe with a diameter of 0.5 mm was attached to the point of divergence of the MCA, and CBF was measured continuously in the parietal lobe using a laser Doppler flowmeter (ALF 21, Advance Co., Ltd, Tokyo), in conjunction with a PowerLab system (AD Instruments, CA, USA).

MRA analysis

MRA was performed as previously described [17], with minor modifications. Mice were anesthetized with pentobarbital and subjected to micro-MRI scans using a vertical bore 9.4 T Bruker AVANCE 400WB imaging spectrometer with a 250 mT/m actively shielded microimaging gradient insert (Bruker BioSpin GmbH, Ettlingen, Germany) [17]. A 25-mm resonator was used for signal excitation and detection. The depth of anesthesia was monitored with a breathing sensor, and was maintained with 0.5 to 1.5% isoflurane in air (2 l/min flow rate). Two-dimensional horizontal MRA images were acquired by using a method derived from gradient-echo pulse sequence with flow compensation. The scans were performed with the following imaging parameters: $TR = 50.0$ ms; $TE = 5.0$ ms; flip angle $= 25°$; matrix $= 256 \cdot 256$; field of view $= 2 \cdot 2$ cm^2; number of slices $= 40$; slice thickness $= 0.05$ mm; and total imaging time $= 51$ min (10 averages). Angiograms were obtained by generating maximum intensity projections using Paravision software (Bruker BioSpin GmbH). Basilar arterial vascular area was measured on the perpendicular section of the vessel using OSIRIX software, and mean vascular dimension was determined as the average of 7 segments in the measured area (Fig. 3A).

Ovariectomy and E2 implantation

Ovariectomies were performed 4 months after birth using standard surgical procedures. MRA was carried out 2 weeks after OVX surgery on 4 month-old female $M5R^{+/+}$ and $M5R^{-/-}$ mice. For transient E2 treatment experiments, 1 μg E2 was injected into the tail vein. For the chronic administration (3 weeks) of estrogen pellets (steady-release pellet of an 0.1 mg 17β-estradiol pellet) to adult male mice, a small incision was made in the dorsal neck region for the insertion of the hormone pellet (Innovative Research) to maintain plasma estrogen levels ranging from 250

110

to 260 pg/mL, and the incision was closed with a wound clip under anesthesia. The doses used in these experiments were chosen based upon their ability to generate physiological serum concentrations [19]. Estrogen was below the level of detection prior to E2 treatment of male mice.

Cell culture

The conditionally immortalized mouse brain capillary endothelial cell line (TM-BBB) was performed as previously described [61]. The culture medium used consisted of DMEM (Gibco, Carlsbad, CA) supplemented with 15 µg/ml endothelial cell growth factor (Roche Diagnostics, Indianapolis, IN), 100 U/ml benzylpenicillin potassium, 100 µg/ml streptomycin sulfate, and 10% fetal bovine serum.

Immunoblotting

TM-BBB cells were seeded at a density of 6.5×10^4 cells per dish on collagen type I-coated 35-mm culture dishes (Becton Dickinson). After 48 h of culture, cells were incubated for 24 h in growth factor-free medium followed by 2 h incubation in serum-free fresh medium at 33 °C. TM-BBB cells were incubated at 33 °C with vehicle, bethanechol 100 µM (Bch: MP Biomedicals, Solon, OH) or 17-β-estradiol 10 nM (E2: Sigma Chemical Co.) as indicated. TM-BBB cells were also treated with selective activators of ERα (1,3,5-Tris(4-hydroxyphenyl)-4-propyl-1H-pyrazole; PPT, Sigma), ERβ (DPN, Tocris Bioscience), and GPR30 (G1, MERCK). Cells were rinsed with ice-cold phosphate-buffered saline (PBS) containing 0.5 mM Na3VO4 and then collected in 100 µl of lysis buffer (50 mM Tris-HCl, pH 7.5, containing 150 mM NaCl, 1% Triton X-100, 1% deoxycholate, 0.2 mM Na3VO4, 1 mM EGTA, 0.4 mM EDTA, 1 mg/ml of aprotinin and leupeptin, and 0.1 mg/ml of phenylmethylsulphonyl fluoride). Lysates were centrifuged at 10,000 g for 15 min at 4°C to remove insoluble material and normalized for protein content. Equal amounts of protein (20 µg) were separated by 10% SDS–PAGE, transferred to nitrocellulose membranes (Schleicher & Schuell), probed with rabbit polyclonal phospho-p44/42 MAP kinase antibody or rabbit polyclonal p44/42 MAP kinase antibody (Cell Signaling Beverly, MA). Subsequently, the membranes were incubated with goat anti-rabbit IgG secondary antibodies (PerkinElmer Life Sciences Inc. Boston, MA).

RT-PCR

Total RNA was extracted from tissues derived from TM-BBB using Trizol reagent (GIBCO). After DNase treatment (2 units μl^{-1}; Ambion), total RNA (≈1 µg) was reverse-transcribed by using oligo (dT)16 primers and murine leukemia virus RT (Perkin–Elmer), followed by PCR amplification of a DNA segment specific for each receptor gene (PCR conditions: 98°C for 2 min; 35 cycles of 98°C for 10 sec and 55°C for 30 sec; 72°C for 5 min). For PCR amplification for the ER alpha gene, 5'-TGGCGCTCCATGGAACAC-3' and 5'-CATCTCCAGGAGCAGGTC-3'; ER beta gene, 5'-AAAGC-CAAGAGAACCAGTGGGCAC-3' and 5'-GCCAATCATGTG-CACCAGTTCCTT-3'; GPR30 gene, 5'-ATCTGGATGGCCT-CAGTGTC-3' and 5'-ACTATGTGGCCTGTCAAGGG-3'; M3 receptor gene, 5'-ACCAAGACCACAGTAGCAGTG-3' and 5'-CTCTCTACATCCATAGTCCC-3'; M5 receptor gene, 5'-GTCTCCGTCATGACCATACTCTA-3' and 5'-CCCGTTGT-TGAGGTGCTTCTAC-3'

Nitrite assay

NO production was determined by measuring nitrite accumulation in culture medium using the NO2/NO3 Assay Kit-FX

(Dojindo Laboratories, Kumamoto, Japan) according to manufacturer's instructions. Briefly, TM-BBB cells were seeded at a density of 6×10^4 cells per dish on collagen type I-coated 24 well plates (IWAKI, Chiba, Japan). After 48 h of culture, cells were washed twice with phenol red-free and serum-free MEM (Gibco) followed by incubation in 300 µl of the same medium containing vehicle, Bch or E2. After this incubation period, 300 µl of medium were removed from each well and centrifuged at 1,000 g for 15 min at room temperature. Supernatants (80 µl aliquots) were mixed with 20 µl of Buffer solution (pH 7.6) and 10 µl of fluorescence reagent (2,3-Diaminonaphthalene) solution, followed by incubation for 30 min at room temperature. The reaction was terminated by the addition of 30 µl of Stop solution. Fluorescence was measured using a spectrofluorometer (ARVO MX, PerkinElmer Life Sciences Inc.), with excitation and emission wavelengths set at 355 and 460 nm, respectively

Immunohistochemistry and Golgi staining

Frozen cryosections (15 µm) were treated with 3% H_2O_2, incubated with blocking buffer (PBS containing 0.01% Triton and 1.5% normal goat serum), and incubated overnight at 4°C with primary antibodies. Sections were incubated with secondary antibody in blocking buffer for 1 h at room temperature. The primary antibodies used were anti-GFAP Ab (DAKO), anti-Iba-1 (Wako, Japan), and anti-Mac-2 (American Type Culture Collection, USA). Secondary antibodies were alexa fluor 546 goat anti-mouse IgG (Molecular Probes) and alexa fluor 488 goat anti-rabbit IgG (Molecular Probes). Sections were counterstained with Hoechst (CALBIOCHEM). Golgi staining was performed essentially as described previously [17]

Electron microscopy

For electronmicroscopic observation of astrocytes in the CA3 region of the hippocampus, a $M5R^{-/-}$ mouse and a wild-type control mouse were fixed 2.5% glutaraldehyde and 4% paraformaldehyde. After fixation, the tissue samples were postfixed with 1% (w/v) osmium tetroxide in 0.1 M PB, dehydrated in a graded ethanol series, and embedded in epoxy resin (EPON812, TAAB, Aldermaston, UK). For electron microscopic observations, the brain was sectioned into a series of 100–110 sections (70 nm thick) with an ultramicrotome (EM UC6, Leica, Heidelberg, Germany). Ultrathin sections were stained with uranyl acetate and lead citrate. Electron micrographs recorded on imaging plates through a JEM-1200EX electron microscope (JEOL DATUM LTD., Tokyo, Japan) were scanned and digitized by an FDL 5000 imaging system (Fuji Photofilm, Tokyo, Japan). To reconstruct 3D images of astrocytes, each series was aligned using sEM Align software and edges of astrocytic cytoplasm were traced using IGL Trace software based on ref. [62] (freely available at http://synapse-web.org/tools/reconstruct/reconstruct.stm).

Y-maze test

The Y-maze task was performed essentially as described previously [17].

Statistical Analysis

Data are expressed as mean±SEM. Statistical comparisons of CBF, nitrite, and MRA data were performed using Student's t-test or ANOVA. $p < 0.05$ was considered to be statistically different.

Supporting Information

Figure S1 Gender-specific phenotypic differences in CBF displayed by M5R−/− mice. CBF was measured in the middle

111

cerebral artery and arterioles (MCA). MCA branches were defined in the order from A1 to A3 for classification scheme, described [17]. CBF was measured in the A1 area by laser-Doppler flowmetry. Male M5R−/− mice showed significantly reduced CBF, as compared to male M5R+/+ mice. In contrast, female M5R+/+ and M5R−/− mice displayed similar CBF. OVX female M5R−/− mice showed reduced CBF, similar to male M5R−/− mice. Data are expressed as CBF relative to M5R+/+ (white bars). OVX mice were used for CBF measurements 4 weeks after surgery performed on 4-month-old female M5R−/− and M5R+/+ mice. The numbers given in parentheses under the bars indicate the number of independent experiments (mice). Data are means±SEM. **p<0.001 (vs M5R+/+ mice).
Found at: doi:10.1371/journal.pone.0005159.s001 (11.24 MB DOC)

Figure S2 Gender-specific phenotypic differences displayed by female M5R−/− mice. Relative expression levels, determined by Western blot analysis, of cortical (top panel) and hippocampal (lower panel) glutamate receptor subunits in female M5R−/− and M5R+/+ (=100%) mice, and OVX M5R−/− and OVX M5R+/+ (=100%) mice. The numbers given in parentheses underneath the bars indicate the number of independent experiments (mice). Data represent means±SEM; *p<0.05; **p<0.001.
Found at: doi:10.1371/journal.pone.0005159.s002 (11.24 MB TIF)

Figure S3 PMSG/hCG treatment did not significantly affect the diameter of the basilar artery in male mice. (A) Experimental schedule for PMSG/hCG/E2 treatment experiments. (B) PMSG/hCG treatment did not affect the diameter of the basilar artery during transient or chronic E2 treatment experiments. All studies were carried out with 3 month-old male M5R+/+ and M5R−/− mice (n = 12 per group). Data represent means±SEM; *p<0.05; **p<0.001.
Found at: doi:10.1371/journal.pone.0005159.s003 (9.00 MB TIF)

Figure S4 Male M5R−/− mice exhibit astrocyte activation without migration of microglia. Frozen sections of cerebral cortex and hippocampus were prepared from 4-month-old male M5R+/+ and M5R−/− mice. An E2 tablet (0.1 mg/21 days release) was implanted into neck of each mouse. (A) GFAP immunostaining signals in the hippocampal CA3 region from E2-treated male M5R−/− and M5R+/+ mice vs. non-treated male M5R−/−

mice. Scale bar = 200 μm. (B) E2 treatment of male M5R−/− mice restored wild-type-like GFAP protein expression levels in the hippocampus, as studied by western blotting analysis. E2-treated male M5R+/+ mice showed similar GFAP protein expression levels as non-treated male M5R+/+ mice. Data are means±SEM (n = 8 per group). *p<0.05 (vs M5R+/+ mice). (C) Male M5R−/− mice showed a significantly increased number of GFAP positive cells in the CA3 region of the hippocampus. However, the number of S100β positive astrocytes, a measure of the total number of astrocytes, remained unchanged. Five hippocampal CA3 sections from 5 animals per group were analyzed. Values are means±SE. **p<0.001. (D) Vimentin and neurocan, markers for injured astrocytes, did not show any increase in immunoreactivity in male M5R−/− mice. Scale bar, 1 mm. (E) Leakage of EB in surrounding blood vessels was not detected in cortex and hippocampus of male M5R−/− and M5R+/+ mice. Scale bar, 1 mm.
Found at: doi:10.1371/journal.pone.0005159.s004 (11.24 MB TIF)

Movie S1
Found at: doi:10.1371/journal.pone.0005159.s005 (0.96 MB SWF)

Movie S2
Found at: doi:10.1371/journal.pone.0005159.s006 (1.90 MB SWF)

Movie S3
Found at: doi:10.1371/journal.pone.0005159.s007 (2.04 MB SWF)

Movie S4
Found at: doi:10.1371/journal.pone.0005159.s008 (1.85 MB SWF)

Author Contributions

Conceived and designed the experiments: MY. Performed the experiments: NK RA MK HK TK MM AT YS SI SO. Analyzed the data: TK TH JW. Contributed reagents/materials/analysis tools: TT. Wrote the paper: JW MY.

References

1. Faraci FM, Sigmund CD (1999) Vascular biology in genetically altered mice: smaller vessels, bigger insight. Circ Res 85: 1214–1225.
2. Hotta H, Uchida S, Kagitani F (2002) Effects of stimulating the nucleus basalis of Meynert on blood flow and delayed neuronal death following transient ischemia in the rat cerebral cortex. Jpn J Physiol 52: 383–393.
3. Sato A, Sato Y, Uchida S (2004) Activation of the intracerebral cholinergic nerve fibers originating in the basal forebrain increases regional cerebral blood flow in the rat's cortex and hippocampus. Neurosci Lett 361: 90–93.
4. Furchgott RF, Zawadzki J V (1980) The obligatory role of endothelial cells in the relaxation of arterial smooth muscle by acetylcholine. Nature 288: 373–376.
5. Rosenblum WI (1986) Endothelial dependent relaxation demonstrated in vivo in cerebral arterioles. Stroke 17: 494–497.
6. Huang PL, Huang Z, Mashimo H, Bloch KD, Moskowitz MA, et al. (1995) Hypertension in mice lacking the gene for endothelial nitric oxide synthase. Nature 377: 239–242.
7. Meng W, Ma J, Ayata C, Hara H, Huang PL, et al. (1996) ACh dilates pial arterioles in endothelial and neuronal NOS knockout mice by NO-dependent mechanisms. Am J Physiol 271: H1145–H1150.
8. Sobey CG, Faraci FM (1997) Effects of a novel inhibitor of guanylyl cyclase on dilator responses of mouse cerebral arterioles. Stroke 28: 837–842.
9. Yamada M, Lamping KG, Duttaroy A, Zhang W, Cui Y, et al. (2001) Cholinergic dilation of cerebral blood vessels is abolished in M5 muscarinic acetylcholine receptor knockout mice. Proc Natl Acad Sci U S A 98: 14096–14101.

10. Tayebati SK, Di Tullio MA, Tomassoni D, Amenta F (2003) Localization of the m5 muscarinic cholinergic receptor in rat circle of Willis and pial arteries. Neuroscience 122: 205–211.
11. Hamel E (2004) Cholinergic modulation of the cortical microvascular bed. Prog Brain Res 145: 171–178.
12. Wang SZ, Zhu SZ, el-Fakahany EE (1994) Efficient coupling of m5 muscarinic acetylcholine receptors to activation of nitric oxide synthase. J Pharmacol Exp Ther 268: 552–557.
13. Bonner TI, Young AC, Brann MR, Buckley NJ (1988) The obligatory role of endothelial cells in the relaxation of arterial smooth muscle by acetylcholine. Neuron 1: 403–410.
14. Liao CF, Themmen AP, Joho R, Barberis C, Birnbaumer M, et al. (1989) Molecular cloning and expression of a fifth muscarinic acetylcholine receptor. J Biol Chem 264: 7328–7337.
15. Reever CM, Ferrari-DiLeo G, Flynn DD (1997) The M5 (m5) receptor subtype: fact or fiction? Life Sci 60: 1105–1112.
16. Eglen RM, Nahorski SR (2000) The muscarinic M5 receptor: a silent or emerging subtype? Br J Pharmacol 130: 13–21.
17. Araya R, Noguchi T, Yuhki M, Kitamura N, Higuchi M, et al. (2006) Loss of M5 muscarinic acetylcholine receptors leads to cerebrovascular and neuronal abnormalities and cognitive deficits in mice. Neurobiol Dis 24: 334–344.
18. Shibata M, Ohtani R, Ihara M, Tomimoto H (2004) White matter lesions and glial activation in a novel mouse model of chronic cerebral hypoperfusion. Stroke 35: 2598–603.

112

19. Shibata M, Yamasaki N, Miyakawa T, Kalaria RN, Fujita Y, et al. (2007) Selective impairment of working memory in a mouse model of chronic cerebral hypoperfusion. Stroke 38: 2826–2832.
20. Haynes MP, Sinha D, Russell KS, Collinge M, Fulton D, et al. (2000) Membrane estrogen receptor engagement activates endothelial nitric oxide synthase via the PI3-kinase-Akt pathway in human endothelial cells. Circ Res 87: 677–682.
21. Chen Z, Yuhanna IS, Galcheva-Gargova Z, Karas RH, Mendelsohn ME, et al. (1999) Estrogen receptor alpha mediates the nongenomic activation of endothelial nitric oxide synthase by estrogen. J Clin Invest 103: 401–406.
22. Zivadinovic D, Watson CS (2005) Membrane estrogen receptor-alpha levels predict estrogen-induced ERK1/2 activation in MCF-7 cells. Breast Cancer Res 7: R130–R144.
23. Vivacqua A, Bonofiglio D, Recchia AG, Musti AM, Picard D, et al. (2006) The G protein-coupled receptor GPR30 mediates the proliferative effects induced by 17beta-estradiol and hydroxytamoxifen in endometrial cancer cells. Mol Endocrinol 20: 631–646.
24. Oishi A, Ohmichi M, Takahashi K, Takahashi T, Mori-Abe A, et al. (2004) Medroxyprogesterone acetate attenuates estrogen-induced nitric oxide production in human umbilical vein endothelial cells. Biochem Biophys Res Commun 324: 193–198.
25. Guo X, Razandi M, Pedram A, Kassab G, Levin ER (2005) Estrogen induces vascular wall dilation: mediation through kinase signaling to nitric oxide and estrogen receptors alpha and beta. J Biol Chem 280: 19704–19710.
26. Kim JK, Levin ER (2006) Estrogen signaling in the cardiovascular system. Nucl Recept Signal 4: e013.
27. Xia Y, Krukoff TL (2004) Estrogen induces nitric oxide production via activation of constitutive nitric oxide synthases in human neuroblastoma cells. Endocrinology 145: 4550–4557.
28. Ohtsuki S, Tachikawa M, Takanaga H, Shimizu H, Watanabe M, et al. (2002) The blood-brain barrier creatine transporter is a major pathway for supplying creatine to the brain. J Cereb Blood Flow Metab 22: 1327–1335.
29. Prossnitz ER, Arterburn JB, Smith HO, Oprea TI, Sklar LA, et al. (2008) Estrogen Signaling through the Transmembrane G Protein-Coupled Receptor GPR30. Annu Rev Physiol 70: 165–190.
30. Haas E, Meyer MR, Schurr U, Bhattacharya I, Minotti R, et al. (2007) Differential effects of 17beta-estradiol on function and expression of estrogen receptor alpha, estrogen receptor beta, and GPR30 in arteries and veins of patients with atherosclerosis. Hypertension 49: 1358–1363.
31. Grossini E, Molinari C, Mary DA, Uberti F, Caimmi PP, et al. (2008) Intracoronary genistein acutely increases coronary blood flow in anesthetized pigs through β-adrenergic mediated nitric oxide release and estrogenic receptors. Endocrinology 149: 2678–2687.
32. Khurana S, Yamada M, Wess J, Kennedy RH, Raufman JP (2005) Deoxycholyltaurine-induced vasodilation of rodent aorta is nitric oxide- and muscarinic M3 receptor-dependent. Eur J Pharmacol 517: 103–110.
33. Lamping KG, Wess J, Cui Y, Nuno DW, Faraci FM (2004) Muscarinic (M) receptors in coronary circulation: gene-targeted mice define the role of M2 and M3 receptors in response to acetylcholine. Arterioscler Thromb Vasc Biol 24: 1253–1258.
34. Gao X, Dluzen DE (2001) Tamoxifen abolishes estrogen's neuroprotective effect upon methamphetamine neurotoxicity of the nigrostriatal dopaminergic system. Neuroscience 103: 385–394.
35. Mellergard YB, Ouyang BK, Siesjo (1993) Intracellular pH regulation in cultured rat astrocytes in CO2/HCO3($-$)-containing media. Exp. Brain Res 95: 371–380.
36. Jung YW, Choi IJ, Kwon TH (2007) Altered expression of sodium transporters in ischemic penumbra after focal cerebral ischemia in rats. Neurosci Res 59: 152–159.
37. Dodel RC, Du Y, Bales KR, Gao F, Paul SM (1999) Sodium salicylate and 17β-estradiol attenuate nuclear transcription factor NF-kappaB translocation in cultured rat astroglial cultures following exposure to amyloid Aβ (1–40) and lipopolysaccharides. J Neurochem 73: 1453–1460.
38. Mor G, Nilsen J, Horvath T, Bechmann I, Brown S, et al. (1999) Estrogen and microglia: A regulatory system that affects the brain. J Neurobiol 40: 484–496.
39. Saria A, Lundberg JM (1983) Evans blue fluorescence: quantitative and morphological evaluation of vascular permeability in animal tissues. J Neurosci Methods 8: 41–49.
40. Yang SH, Shi J, Day AL, Simpkins JW (2000) Estradiol exerts neuroprotective effects when administered after ischemic insult. Stroke 31: 745–749.
41. McCullough LD, Alkayed NJ, Traystman RJ, Williams MJ, Hurn PD (2001) Postischemic estrogen reduces hypoperfusion and secondary ischemia after experimental stroke. Stroke 32: 796–802.
42. Yong Y, Xie HJ, Zhang YF, Yang QD, Liao DF, et al. (2005) 17beta-estradiol potentiates ischemia-reperfusion injury in diabetic ovariectomized female rats. Brain Res 1054: 192–199.
43. Santizo RA, Anderson S, Ye S, Koenig HM, Pelligrino DA (2000) Effects of estrogen on leukocyte adhesion after transient forebrain ischemia. Stroke 9: 2231–2235.
44. Jia J, Guan D, Zhu W, Alkayed NJ, Wang MM, et al. (2009) Estrogen inhibits Fas-mediated apoptosis in experimental stroke. Exp Neurol 215: 48–52.
45. Karas RH, Patterson BL, Mendelsohn ME (1994) Human vascular smooth muscle cells contain functional estrogen receptor. Circulation 89: 1943–1950.
46. Kim-Schulze S, McGowan KA, Hubchak SC, Cid MC, Martin MB, et al. (1996) Expression of an estrogen receptor by human coronary artery and umbilical vein endothelial cells. Circulation 94: 1402–1407.
47. Chambliss KL, Shaul PW (2002) Estrogen modulation of endothelial nitric oxide synthase. Endocr Rev 23: 665–686.
48. Razandi M, Pedram A, Merchenthaler I, Greene GL, Levin ER (2004) Plasma membrane estrogen receptors exist and functions as dimmers. Mol Endocrinol 18: 2854–2865.
49. Syková E, Mazel T, Hasenöhrl RU, Harvey AR, Simonová Z, et al. (2002) Learning deficits in aged rats related to decrease in extracellular volume and loss of diffusion anisotropy in hippocampus. Hippocampus 12: 269–279.
50. Rehncrona S (1985) Brain acidosis. Ann Emerg Med 14: 770–776.
51. Yao H, Ginsberg MD, Eveleth DD, LaManna JC, Watson BD, et al. (1995) Local cerebral glucose utilization and cytoskeletal proteolysis as indices of evolving focal ischemic injury in core and penumbra. J Cereb Blood Flow Metab 15: 398–408.
52. Orlowski J, Grinstein S (2004) Diversity of the mammalian sodium/proton exchanger SLC9 gene family. Pflugers Arch 447: 549–565.
53. Ma E, Haddad GG (1997) Expression and localization of Na+/H+ exchangers in rat central nervous system. Neuroscience 79: 591–603.
54. Slezak M, Pfrieger FW (2003) New roles for astrocytes: regulation of CNS synaptogenesis. Trends Neurosci 26: 531–535.
55. Wang X, Lou N, Xu Q, Tian GF, Peng WG, et al. (2006) Astrocytic Ca2+ signaling evoked by sensory stimulation in vivo. Nat Neurosci 9: 816–823.
56. Haydon PG (2001) GLIA: listening and talking to the synapse. Nat Rev Neurosci 2: 185–193.
57. Ullian EM, Sapperstein SK, Christopherson KS, Barres BA (2001) Control of synapse number by glia. Science 291: 657–660.
58. Woolley CS, McEwen BS (1994) Estradiol regulates hippocampal dendritic spine density via an N-methyl-D-aspartate receptor-dependent mechanism. J Neurosci 14: 7680–7687.
59. Green PS, Bishop J, Simpkins JW (1997) 17 β-estradiol exerts neuroprotective effects on SK-N-SH cells. J Neurosci 17: 511–515.
60. Dubal DB, Zhu H, Yu J, Rau SW, Shughrue PJ, et al. (2001) Estrogen receptor alpha, not beta, is a critical link in estradiol-mediated protection against brain injury. Proc Natl Acad Sci USA 98: 1952–1957.
61. Hosoya K, Tetsuka K, Nagase K, Tomi M, Saeki S, et al. (2000) Conditionally immortalized brain capillary endothelial cell lines established from a transgenic mouse harboring temperature-sensitive simian virus 40 large T-antigen gene. AAPS PharmSci 2: E27.
62. Cooney JR, Hurlburt JL, Selig DK, Harris KM, Fiala JC (2002) Endosomal compartments serve multiple hippocampal dendritic spines from a widespread rather than a local store of recycling membrane. J Neurosci 22: 2215–2224.

113

Review Article

Amyloid-β, Tau, and Dementia

Akihiko Takashima*
Laboratory for Alzheimer's Disease, RIKEN Brain Science Institute, Wako, Saitama, Japan

Abstract. Alzheimer's disease (AD) is clinically characterized as a progressive dementia starting with memory dysfunction and characterized pathologically as neurodegeneration accompanied by deposition of amyloid-β, neurofibrillary tangles, and neuronal loss. AD research has endeavored to explain the clinical symptoms of AD through pathological changes and to develop various therapies for AD. Fulfillment of these goals, however, remains on the horizon. In this article, I review the relationship between neuropathological changes that occur in the brain and clinical progression of AD, and propose a hypothesis that brain aging, characterized by neurofibrillary tangles in entorhinal cortex, is pre-requisite for development of AD.

Keywords: Amyloid-β, dementia, tau

INTRODUCTION

Although the progression of the symptoms of Alzheimer's disease (AD) varies across individuals, symptoms manifested during early stages of the disease appear to be similar. According to the Global Deterioration Scale (GDS) [1], a psychological instrument that rates cognitive deterioration, AD can be divided into seven stages. Stage 1 is characterized by the absence of cognitive decline. Individuals in this stage exhibit no problems in daily living. Stage 2 is characterized by very mild cognitive decline. Individuals in this stage forget names and locations of objects and may have trouble finding words – all behaviors that are dependent on the functions of the entorhinal cortex hippocampus and part of the prefrontal cortex. Stage 3 is characterized by mild cognitive decline. Individuals in this stage face difficulties in traveling to new locations and in handling problems at work. These behaviors also depend on the entorhinal cortex and hippocampus and part of the prefrontal cortex. Stage 4 is characterized

by moderate cognitive decline. Individuals in this stage have difficulty completing complex tasks, that depend on intact prefrontal cortex function. Stages 5 to 7 are characterized by moderately severe cognitive decline to very severe cognitive decline. In addition to manifesting behaviors typical of entorhinal cortical, hippocampal, and prefrontal cortical dysfunction, individuals in these later stages of AD require help in daily living, which is indicative of dysfunction of the basal ganglia, amygdala, and association cortices. Thus, memory formation and recall, abilities that depend on entorhinal cortical, hippocampal, and prefrontal cortical function, are the first to show impairment during the early stages of cognitive decline in AD. Subsequently, impairment appears in other brain areas, leading to dementia. How can the pathological hallmarks of AD – amyloid-β (Aβ) deposition and neurofibrillary tangle (NFT) formation – explain the progression of AD from memory impairment to dementia?

AMYLOID-β

Amyloid-β protein precursor (AβPP) mutations have been found in cases of familial AD (FAD). These mutations increase Aβ production, including the longer

*Address for correspondence: Akihiko Takashima, Ph.D., Laboratory for Alzheimer's Disease, Brain Science Institute, RIKEN, 2-1 Hirosawa, Wako-shi, Saitama 351-0198, Japan. Tel.: +81 48 467 9704; Fax: +81 48 467 5916; E-mail: kenneth@brain.riken.go.jp.

form of Aβ or fibrillogenic Aβ [2,3], which when aggregated induces neuronal death. Thus, Aβ is thought to be one cause of AD. In 1991, Hardy and Higgins proposed the Aβ hypothesis: Aggregated Aβ affects neurons and induces NFT formation and neuronal loss, eventually leading to dementia [4–6]. *In vitro* studies partly support this idea. Aggregated Aβ, excluding amorphous Aβ, for example, induces neuronal death in primary hippocampal neuronal cultures accompanied by hyperphosphorylation of tau [7–9]. However, overexpression of AβPP with the FAD mutation in mouse brain causes Aβ deposition but not NFT formation and clear neuronal loss, even though these mice show impaired spatial memory formation [10–12]. The apparent disparity in the effects of aggregated Aβ on neurons *in vitro* and *in vivo* may stem from the possibility that different species of aggregated Aβ exist.

When Yankner's group first reported that Aβ induces neurotoxicity, they used in their experiments "aged Aβ," which forms Congo red-positive, thioflavin-positive fibrils [9,13]. Therefore, Aβ aggregates having β-pleated sheets represent a potent neurotoxic form of Aβ aggregate. However, the possibility that "aged Aβ" contains aggregate forms other than fibrils cannot be excluded. Similar findings were also observed with the aggregation of other peptides, such as amylin [14] and all D-enantiomers of Aβ peptide [15]. These observations suggest that Aβ aggregates that take on a β-pleated sheet conformation induce cytotoxicity. This type of cytotoxicity may not be mediated by specific receptors, however, because aggregated D-enantiomers of Aβ peptide [15] also cause neuronal death.

Other studies showed that protofibrils of Aβ are more toxic than mature fibrils, because mature fibrils have a reduce ability to associate with cell surface membranes [16]. Recent studies have claimed that oligomeric Aβ [17–19], such as amyloid-β-derived diffusible ligand (ADDL) or so-called Aβ56*, represents the toxic species of Aβ that aggregates in AD brains. This small soluble form of oligomeric Aβ aggregate induces neuronal death in organotypic neuronal cultures, and significantly inhibits LTP induction [20–22]. More recently, dimerized Aβ has been reported to be the smallest oligomer capable of inhibiting synaptic plasticity, leading to memory impairment [19,23]. Thus, with the exception of monomeric forms, Aβ affects neurons, leading to neuronal death and impairment of synaptic plasticity [23,24].

Since mice overexpressing the AβPP FAD mutation show impaired hippocampal LTP as well as memory deficits similar to those seen in AD, it is conceivable

that soluble Aβ oligomers may be involved in the neural dysfunction that occurs in AD brains. Although the role of Aβ oligomers in the clinical progression of AD remains unclear, animal models based on the Aβ aggregation hypothesis (e.g., mice overexpressing the AβPP FAD mutation) continue to be used for developing therapeutic drugs for AD. In Aβ immunotherapy, immunizing a mouse against Aβ42 prevents Aβ deposition and memory impairment [25–30], suggesting that Aβ immunotherapy can remove Aβ oligomers, which seems to be a cause of memory deficits. Clinical trials involving the immunization of AD patients with Aβ42, however, did not produce the same results as the mouse model. While immunotherapy resulted in the removal of Aβ plaques in AD brains, the removal of plaques failed to halt progressive neurodegeneration [31]. Although there was wide variation in Aβ load and pathology in the immunized group, Braak tau stage was V to VI, and Mini-Mental Status Examination (MMSE) score declined from around 17 in average score to nearly 0. There are several reasons why Aβ immunotherapy was ineffective in treating AD patients. However, just because Aβ immunotherapy was ineffective in treating AD patients, we cannot conclude that Aβ does not play a role in AD. Indeed, all of the causative genes for FAD affect Aβ generation, and Aβ oligomers induce synaptic dysfunction in brain, indicating that Aβ does play some role in AD neuropathology. Since AβPP-overexpressing mice do show memory impairment without tau pathology and neuronal loss [32], some of the tau changes that occur before NFT formation may be involved in memory impairment. These changes, however, may be insufficient to promote NFT formation and neuronal loss. Interestingly, reducing tau levels in AβPP-overexpressing mice prevents Aβ-induced memory deficits [32]. Therefore, pathological changes in tau, which lead to NFT formation and neuronal loss, may be key to understanding why Aβ removal failed to halt the clinical course of AD in humans.

TAU

Intraneuronal fibrillar depositions of hyperphosphorylated tau protein form NFTs, a hallmark of AD. Increasing deposition of tau is found in the brain during aging and in some neurological disorders, such as Pick's disease, progressive supranuclear palsy, and frontotemporal dementia. Neuronal death is observed in the same brain regions as NFTs, and both neuronal

death and NFTs correlate with the duration and severity of illness in AD, although the amount of neuronal death is many times more than the number of NFTs [33]. Recently, a tau mutation was identified as the causal factor in frontotemporal dementia parkinsonism-17 (FTDP-17), a dementing disease characterized by NFT formation and neuronal loss [34–39]. The elucidation of mutated tau in FTDP-17 conclusively demonstrated that tau dysfunction or abnormality alone could induce neurodegeneration characterized by NFTs and neuronal death, leading to clinical dementia similar to that found in AD.

Braak and colleagues classified the progression of AD into six stages based on the distribution of NFTs in the brain [40]. In Braak stage I, NFTs are formed in the transentorhinal cortex and the CA1 region of the hippocampus. The number of NFTs increases in Braak stage II, and Braak stages I and II together are called the transentorhinal stage. Braak stages I and II are classified as normal aging. In Braak stages III and IV, called the limbic stage, many "ghost" tangles appear in the entorhinal cortex, and NFTs are found throughout the entire limbic system, including hippocampal regions CA1–4 and the amygdala. In the limbic stage, patients show various AD-specific symptoms, such as memory impairment, reduced spatial cognition, and reduced desire as a result of neural dysfunction in the limbic system. In Braak stages V and VI, called the isocortical stage, NFTs are present in the cerebral cortex, resulting in impaired neural function and dementia. This increasing spread of NFTs into cerebral cortex correlates with increasing impairment of brain function. Samuel and colleagues reported that the number of NFTs in CA1, subiculum, and CA4 of the hippocampal formation correlate with the degree of dementia, and also that synapse loss in dentate gyrus, CA2/3, and CA4 strongly correlates with the degree of dementia [41]. Therefore, the distribution of NFTs is thought to correlate with disease progression in AD, and synapse loss is key to understanding dementia in AD. Others have also shown a link between NFT formation and synaptic dysfunction. For example, NFT-bearing neurons have reduced GAP-43 mRNA and show synapse loss [42]. Moreover, axoplasmic transport may be impaired in NFT-bearing neurons, because they contain diminished and twisted microtubules [41]. These observations indicate that synapse loss may occur through the impairment of axonal transport.

Impairment of axonal transport through tau was first suggested by data from in vitro studies. Hirokawa's group and Mandelkow's group reported that tau overex-

pression inhibits kinesin-mediated fast transport [43–45]. This was corroborated by single molecule analysis. Dixit and colleagues showed that kinesin detaches from microtubules at patches of bound tau that consist of about 10 molecules of tau [46]. Increasing monomeric tau concentrations by 20-fold above physiological tau concentrations, however, fails to affect axonal transport in squid axon [47]. Taken together, these findings indicate that aggregated tau on microtubules, not monomeric tau, may promote inhibition of axonal transport.

However, there are discrepancies in the findings of reports that used human wild-type tau-overexpressing mice to assess the effects of tau on axonal transport. Ishihara and colleagues indicated that 5–10-fold overexpression of shortest human tau over endogenous tau concentrations inhibits axonal transport [48], whereas Nixon's group reported that 4-fold overexpression of human tau does not inhibit axonal transport [49]. Therefore, it is possible that the effect of tau on axonal transport in vivo may depend on the level of tau overexpression. However, because no evidence exists to show that tau overexpression occurs in the brains of those with AD, it remains unclear whether a tau-induced impairment of axonal transport contributes to the dementia characteristically observed in AD.

An FTDP-17 mouse model that displays age-related NFTs, neuronal death, and behavioral deficits may shed light on how tau induces neuronal dysfunction. These mice overexpress P301L mutant tau under the regulation of a tetracycline-inducible promoter. Although inhibiting mutant tau overexpression in these mice blocks neuronal death and improves memory, NFTs continue to form [50], indicating that NFTs may not be responsible for neuronal death. Recent observations that NFT-bearing neurons contain activated caspase but do not undergo acute apoptosis [51] suggest that NFTs are not themselves toxic, but instead that the mechanism of NFT formation is shared by the process underlying neuronal death and neuronal dysfunction. The relationship between neuronal loss and memory dysfunction in the P301L mutant tau mouse model remains unclear. However, the key to understanding tau-induced neuronal dysfunction may be found by examining how NFTs are formed.

In order to form tau fibrils, tau monomers first bind together through disulfide bonds and SDS-resistant interactions to form tau oligomers, which are not visible under atomic force microscopy (AFM). Forty tau molecules bind together forming a β-sheet structure. These 40-tau aggregates appear granular in shape un-
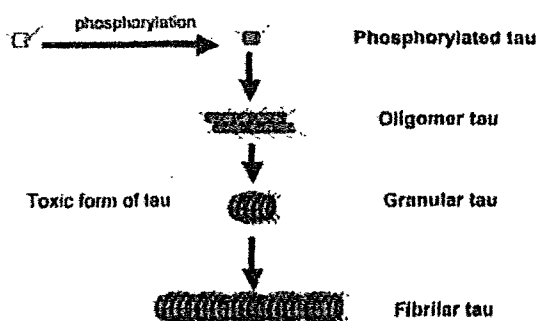
Granular tau is a toxic species of tau aggregate

Fig. 1. Mechanism of tau filament formation. Tau becomes highly phosphorylated and detaches from microtubules. Before fibril formation, phospho-tau forms oligomeric tau, which cannot be visualized through AFM. After attaining a β-sheet configuration, oligomeric tau turns into a granular form of tau aggregate, which is visible in AFM. Granular tau sticks together to form tau fibrils. This cascade -- phosphorylated tau formation to granular tau formation – may contribute to synaptic loss and neuronal loss.

der AFM. Accumulations of granular tau stick together to form tau fibrils. Therefore, before tau fibrils are formed, tau forms two different kinds of aggregates: tau oligomers, which are not detectable by thioflavin T staining or by AFM, and granular tau oligomers, which are detectable by AFM (Fig. 1) [52]. Increased levels of granular tau oligomer are found in frontal cortex from Braak stage I brains [53]. NFTs, however, do not appear in frontal cortex until Braak stage V, suggesting that the increase in granular tau oligomer formation precedes NFT formation. We found that aged transgenic (Tg) mice that express wild-type tau show memory impairment accompanied by synapse loss and accumulation of hyperphosphorylated tau, but without NFT formation in entorhinal cortex. Thus, hyperphosphorylated tau aggregation and corresponding synaptic dysfunction may occur far before NFTs form.

There are several ways to inhibit tau aggregation formation. Before tau aggregation occurs, tau is modified by hyperphosphorylation. An average of eight phosphate molecules are incorporated into one tau molecule in AD brains, while two phosphate molecules are incorporated into one tau molecule in normal adult brains. Therefore, one potential therapy for AD may involve using kinase inhibitors to inhibit tau hyperphosphorylation. Preliminary work toward this end has shown that tau kinase inhibitors block NFT formation in tau Tg mice [54,55]. Development of tau kinase inhibitors as well as their clinical testing is still underway.

Another known tau aggregation inhibitor is methylthionium chloride, or so-called methylene blue. During the 2008 International Conference on Alzheimer's Disease (ICAD), methylthionium chloride (Rember™) treatment was reported to significantly block the progression of cognitive decline in mild-to-moderate AD patients who took the drug for at least 19 months [56]. This finding indicates that tau aggregation is closely related to neuronal dysfunction.

TAU AND Aβ

In clinical studies, Aβ immunizations failed to block the progression of cognitive decline in patients with clinically diagnosed AD, even though Aβ deposition was absent [31]. On the other hand, a tau aggregation inhibitor significantly blocked the progression of cognitive decline in AD patients [56]. These findings indicate that aggregated tau, excluding tau fibrils, may more directly affect neuronal function than oligomeric Aβ. Because inhibiting mutant tau overexpression in these mice blocks neuronal death and improves memory, but NFTs continue to form [50] and Aβ deposit was not toxic, Aβ plaque and NFT, which are pathological marker of AD, may not be a direct cause of neurodegeneration. The intermediate form of tau and Aβ fibril rather play an important role in neurodegeneration of AD. NFT and Aβ deposition may be a bystander and work as a protector for toxic intermediate of Aβ and tau fibril [57]. In AβPP Tg mice, memory impairment is mediated through tau, because the offspring resulting from the crossbreeding of AβPP Tg mice with tau KO
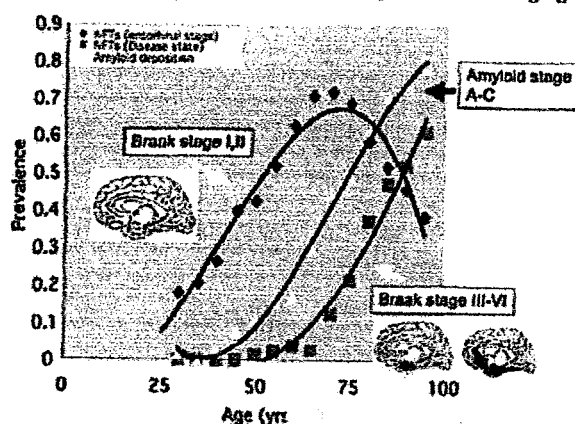
Relationship between Aβ deposition and NFT formation during aging

Fig. 2. Relationship between Aβ deposition and NFT formation. On the basis of Braak's report [2], we calculated the prevalence of NFTs during Braak stages I and II, and the prevalence of Aβ deposition and NFTs during Braak stages III-IV (dementia), and plotted these figures according to different age groups.

mice do not show memory impairment [32]. Therefore, pathological changes in tau may represent the executing factor for neurodegeneration that affects neuronal function. Oligomeric Aβ, on the other hand, may represent the initiating factor for neurodegeneration that triggers certain changes in tau (e.g., tau hyperphosphorylation and several steps of tau aggregation). Once tau changes begin, neuronal dysfunction occurs sequentially, starting with synapse loss resulting from the formation of hyperphosphorylated tau, which leads to neuronal loss and NFT formation resulting from some sort of aggregated form of tau. Consequently, neuron loss and NFT formation may lead to fatal functional loss.

Observations on the pathology of AD brains have revealed that a chronological relationship exists between oligomeric Aβ and tau. Figure 2 outlines the relationship between NFTs and Aβ deposition during aging. During the transentorhinal stage, Aβ deposition varies, sometimes with no Aβ deposition. The prevalence of the transentorhinal stage increases with age, independent of Aβ deposition (which peaks at approximately 75 years of age, and then decreases due to the spread of NFTs into other brain regions). However, the prevalence of NFTs in Braak stages III–VI increases after Aβ deposition. Thus, NFT formation in normal aging is not dependent on Aβ deposition. After NFTs form in the entorhinal cortex, the spread of NFTs to the limbic system and neocortex, as seen in AD, may require Aβ deposition. Thus, the chronology of the pathological changes seen in AD seems to start with the formation of NFTs – perhaps caused by aging factors, such as oxidative stress – in the entorhinal cortex independent of

oligomeric Aβ level. Increasing oligomeric Aβ level, which leads to Aβ deposition and triggers the spread of NFTs into the limbic system and neocortex, follows formation of NFT in entorhinal cortex.

During aging, NFTs are formed first in entorhinal cortex as a result of normal aging. At this time, tau in other brain regions may also undergo some pre-pathological changes. This premise is consistent with the increased granular tau aggregation observed in the prefrontal cortex at Braak stage I [52,53], a stage defined as a state of normal aging, which means no sign of dementia in clinical diagnosis. During this stage, some functional impairment in the entorhinal cortex and prefrontal cortex may exist. However, the effect of this limited neural impairment on brain function may be compensated by the other neural circuit. Oligomeric Aβ further accelerates the formation of granular tau aggregates, leading to NFT formation in the limbic system and neocortex, accompanied by synapse loss and neuron loss. The compensation mechanism may not be rescued anymore once neurodegeneration has spread throughout the entire brain. The synaptic loss in the limbic system and neocortex that occurs as a result of pathological changes in tau represents one cause of cognitive decline. Subsequent neuronal loss leads to a fatal loss of neuronal function, leading to irreversible dementia (Fig. 3).

CONCLUSIONS

Aβ initiates the tau aggregation cascade and may accelerate brain dysfunction. In normal aging, the ag-